Gel Stability in Waves:

breakage, behaviour, and implications for oil spill remediation

by

Richard Joseph Cunningham

B.A.Sc., The University of Waterloo, 2018

A THESIS SUBMITTED IN PARTIAL FULFILLMENT OF
THE REQUIREMENTS FOR THE DEGREE OF

MASTER OF APPLIED SCIENCE

in

The Faculty of Graduate and Postdoctoral Studies

(Civil Engineering)

THE UNIVERSITY OF BRITISH COLUMBIA

(Vancouver)

July 2020

The following individuals certify that they have read, and recommend to the Faculty of Graduate and Postdoctoral Studies for acceptance, the thesis entitled:

Gel Stability in Waves: breakage, behaviour, and implications for oil spill remediation

submitted by Richard Joseph Cunningham in partial fulfillment of the requirements for

the degree of Master of Applied Science

in Civil Engineering

Examining Committee:

Gregory A Lawrence, Professor, Civil Engineering, UBC
Supervisor

Michael Isaacson, Professor, Civil Engineering, UBC
Supervisory Committee Member

Abstract

While oil spills are becoming less common, they are an ever-present threat associated with use of petroleum. New developments in chemistry have brought gellants back into the spotlight as a promising spill remediation technique. These chemicals change the material properties of spilled oil, making it more solid. This could help prevent the spreading or weathering of spilled oil, extending the window-of-opportunity available for remediation. While oil-gelling technology shows great promise, the behaviour of surface gels subject to linear ocean waves has not yet been investigated. Determining what wave conditions result in the breakup of a gel layer could help predict the utility of these technologies in the field. This study adopts an experimental perspective to provide insight into the behaviour of gels subjected to wave action, specifically addressing the stretching induced by spatially-variable velocity gradients.

Bottom-of-tank experiments were designed to allow the isolation of wave-induced stretching effects from wave-induced bending. In these experiments, a dense gel (gelatin) was placed on the bottom of a wave tank and constrained vertically. As particle orbits in a shallow-water wave decay vertically with depth, this is an effective means of applying the same spatial velocity gradients that would be observed on the water surface. Analytical models were developed to describe the response of a viscoelastic gel to periodic, spatially-variable velocity gradients for Maxwell and Kelvin-Voigt materials. The analytical models matched experimental data in terms of trend, but under-predicted strain by a constant factor. Ultimately, gel breakage was determined to be related to peak stress across the gel's cross-section. By connecting breaking criteria in monochromatic, linear waves from tank tests to real-world conditions, this project provides an initial perspective on when wave-induced stretching alone could cause the fracture of a marine surface gel.

Lay summary

Oil spills are a problem. Many remediation techniques don't work if response isn't quick enough. Gellants, which make a spill more solid, could be useful to help preserve an oil slick for further remediation. Unfortunately, until now, there was scant research into how these materials behave in the real world. This thesis uses experiments to study how gels interact with the spatially variable movement of water in ocean waves and develops analytical models to describe these interactions. By putting a gel on the bottom of a wave tank, we can isolate these wave-induced stretching effects from bending. Gel breakage occurs above a certain threshold stress. It is shown that wave-induced stretching in real-world waves could potentially lead to the breakage of a marine surface gel even without other forcing mechanisms.

Preface

This thesis is the original and, at the time of submission, unpublished work of the author, Richard Cunningham. Any figures adapted from existing literature are noted as such in their captions. All experimental work in this thesis was designed and conducted by the author using pre-existing wave tanks at BC Research Inc. and the University of British Columbia. All coding was completed in MATLAB by the author. Guidance in the preparation of oil gels was provided by the team at BC Research Inc., though the specific protocols used were developed by the author. Instruction for the use of laboratory equipment was provided by laboratory technicians at BC Research Inc. and the University of British Columbia.

Table of Contents

Appendices

List of Tables

List of Figures

List of Symbols and Abbreviations

General and Experimental

α	Strain phase
C_O	Open fraction of mesh
g	Local acceleration due to gravity
L^*	Non-dimensional half-length
t	Time since start of experiment

Material Properties and Rheology

δ	Phase angle
E	Young's modulus of elasticity
E^*	Complex Young's modulus
ε	Tensile strain
G'	Shear storage modulus
G"	Shear loss modulus
G^*	Complex shear modulus
γ	Shear strain
λ_1	Relaxation time
λ_2	Retardation time
μ	Viscous parameter
$\nu_{Poisson}$	Poisson's ratio
σ	Tensile stress
τ	Shear stress

Waves and Water

d	Water depth
$\delta_{(name)}$	Boundary layer thickness (Li, Stokes, or Sumer)
η	Water surface elevation
f	Frequency
H	Wave height
H_{m0}	Significant wave height (momentum formulation)
k	Wave number
L_w	Wave length
μ_w	Dynamic viscosity of water
ν_w	Kinematic viscosity of water
ω	Rotational frequency
ρ_w	Density of water
s	Elevation coordinate, bed elevation as baseline
T	Wave period
T_p	Wave period associated with peak of wave spectrum
u	Water velocity
u_*	Friction velocity of wind over water
U	Peak water velocity adjacent to gel (neglecting boundary layer)
U_{10}	Wind speed at an elevation of 10 m above still water level
x	Lateral coordinate from arbitrary release point
z	Elevation coordinate, still water level as baseline

Gels

a	Crack length
d_g	Thickness of the gel (or plate)
F	Force experienced by gel (or plate)
L_g	Length of gel (or plate)
L_r	Resting length of gel (or plate)
m_g	Mass of gel (or plate)
ρ_g	Density of gel (or plate)
u_g	Velocity of centroid for gel (or plate)
w_g	Width of gel (or plate)
x_g	Lateral location of centroid in gel (or plate)

Acknowledgements

This thesis could not have been completed without the help and expertise of others. Thank you to the team at BC Research Inc., past and present, for funding me and letting me take part in this project.

Thank you to the staff and students at UBC, especially the Environmental Fluid Mechanics group, for both providing laboratory expertise and acting as a sounding board for my ideas. Thanks to Jason Olsthoorn and Ted Tedford for their input, and George Soong and Scott Jackson for their help in the lab. A particularly great thank you to Marjan Zare and Michael Isaacson for taking the time to read through my thesis and suggesting improvements.

Thank you to Mitacs, for helping fund this research.

Thank you to my family, for always being there.

And, most of all, a thank you to Gregory Lawrence for taking me under his wing, providing guidance when my vision wasn't clear, and letting me conduct research which I can call my own.

-

All laboratory work for the production of this thesis was conducted on the traditional territories of the Musqueam, Squamish, Tsleil-Watuth, and Tsawassen nations.

Dedication

To future generations. I hope there are still some wild, unsullied places left for you to enjoy.

Chapter 1

Introduction

While renewable energy sources fulfill a slowly increasing portion of global demand, non-renewable resources, such as oil and coal, continue to dominate energy markets [1]. Global demand for oil products was 100 million barrels per day in 2019, expected to grow by almost one percent annually until 2025 [2]; so long as the world depends on oil, we must deal with the risk associated with its transport. Fortunately, from a global perspective, the number of medium-to-large marine oil spills (> 7 tonnes) from tanker traffic has decreased significantly over time from almost 80 annually in the 1970s to 6.2 spills per year in the 2010s. This has been accompanied by a decrease in total spill volume from 319.5 to 16.4 mega-tonnes per year from these same incidents; however, 91% of spilled oil in the 2010s came from just 10 cases [3]. This is notably excluding non-tanker spills such as the BP Deepwater Horizon disaster in 2010 which released an estimated five million barrels of oil into the Gulf of Mexico, of which only 800 000 barrels[1] (109 kilo-tonnes) were recovered [5]. An average year in Canada sees twelve reported spills of magnitude greater than 4000 L (0.3 tonnes), one of which will be into navigable waters [6]. Evidently, despite great progress, significant oil spills still occur around the world and, as such, spill response must remain a priority.

In Canada, crude oil production in 2018 reached 4.59 million barrels per day, with almost two-thirds from oil sand production. With continued projected demand for Canadian oil products, expansion projects continue to be proposed and approved [7]. One such proposed development which has seen considerable publicity is the Trans Mountain Expansion Project, designed to increase capacity of an existing crude oil pipeline from Edmonton to Burnaby by 590 000 barrels per day [7]. Bitumen, the crude produced in the Canadian oil sands, can not be transported via pipeline in its raw form. Its viscosity must first be decreased by another another fluid, called a diluent. The combined material is termed “dilbit” or, if the diluent is a synthetic chemical, “synbit” [8]. Conventional spill response mea-

[1] Unit of energy. 1640 liters = 1 barrel of oil equivalent = 0.1367 tonne oil equivalent = 6.119 Giga-Joules [4]

sures are generally unable to provide effective cleanup of dilbit [8], so it is of great importance to investigate alternatives.

Regulation around spill response is present at all scales. The International Convention on Oil Pollution Preparedness, Response and Co-operation is an example of international regulation in this area, and has been joined by over 100 countries. The plan, which first entered into effect in 1995, contains provisions on preparedness, response, and international co-operation, with items ranging from establishment of national preparedness systems to basic reporting requirements to documents carried onboard ships [9]. In Canada, a number of organizations are involved in oil spill response planning at both federal and provincial levels. From a federal standpoint, spills are primarily the responsibility of Transport Canada and the Canadian Coast Guard. Transport Canada oversees development and enforcement of regulations and standards, spill prevention and monitoring, and post-spill reporting. The Canadian Coast Guard's responsibilities are focused on spill management, and spill response is delegated to specialized agencies [10]. Province-level planning is focused on providing additional expertise and response capability [11].

1.1 Oil in the Environment

The many severe and negative effects of oil spills on the environment are explored in a number of oil spill texts [6, 9]. Impacts may be acute, occurring after only a short exposure, or chronic, taking prolonged periods to develop. Some of the most stunning post-spill visuals are of oiled birds. Contact with an oil slick will cause feathers to lose both insulation properties and water resistance, potentially leading to a bird's death; oil in a marine mammal's fur has a similar effect [9], which is particularly lethal for younger individuals [6]. Oil has also been shown to cause eye damage in seals, sea lions, and walruses [6]. Fish are impacted in a number of ways: oil is particularly toxic to fish eggs and larvae, but fish species will also be effected by the loss of plankton associated with an oiled water surface [9]. For humans, worry over fire and explosion should be accompanied by concern over exposure to volatile, carcinogenic aromatic hydrocarbons [9].

Oil products do not remain on the ocean's surface unchanged, but develop over time. This change, termed "weathering", is caused by several processes: spreading, evaporation, dissolution, dispersion, emulsification, photo-oxidation, sedimentation, and biodegradation [12]. These processes occur on a range of timescales extending from seconds to months or years, with the importance of

each waxing and waning over time [12, 13]. As the maximum response time for remediation is 240 hours, set by Transport Canada, many weathering experiments end after 10 days [13]. This, of course, assumes that all oil will have been cleaned up by that point - which may be unachievable for large spills. Active remediation continued for years following the BP Deepwater Horizon disaster [14].

Oil spreading refers to an increase in spill surface area under the influence of gravity and surface tension [12, 15], though slicks may also elongate due to the resurfacing of dispersed oil particles [16]. Spreading is of greatest importance immediately after a spill, with importance waning after a few days [12]. Evaporation also acts on timescales shorter than a week, with 80% of evaporation occurring within the first two days of a spill [6]. It is the most important natural process for removal of oil from the water surface [12]. Oil is made up of many component chemicals which evaporate at different rates. This leaves the heavier, slower-to-evaporate oil components on the water surface, increasing slick viscosity by orders of magnitude [6]. Dissolution also acts on oil component chemicals instead of oil as a whole, but is insignificant in terms of actual oil removal [12]. The second most important natural remediative process is dispersion, overtaking evaporation in importance after the first hundred hours. In this process small droplets of oil break off from a slick and, if small enough to avoid resurfacing, become incorporated into the water column. Like spreading, this does not change the properties of the oil itself [12]. The life of these suspended droplets is not well understood [6], though they will eventually be biodegraded [17].

Emulsification is one of the more bothersome weathering processes for spill remediation. In emulsification, water mixes with the oil to form a "mousse" (named after the dessert, which is also a water-in-oil emulsion). This not only inhibits other forms of weathering but also greatly increases the volume of the slick [12]. Emulsification can occur as early as the day of a spill, with most occurring within the first week. The process can continue to produce more mousse throughout the first year after a spill [12]. Photo-oxidation, like dissolution, does not have large impact spill volume. In this process, solar energy on the extreme upper surface of a slick causes chemical reactions. Unfortunately, many of the reaction products are more toxic than their forbears [12]. Sedimentation involves the incorporation of sediment into the oil bulk [12]. This formation of particle-in-oil emulsions may cause oil to sink, greatly complicating remediation efforts (as was the case for the Kalamazoo fresh-water spill) [18]. The final process, biodegradation, only becomes dominant after the other processes wane in importance. Microbes digest oil on a relatively slow timescale, with biodegradation peaking around a month after a spill.

1.2 Methods of spill remediation

Remediation techniques can be split into two broad categories: physical methods, which typically involve the containment and/or collection of oil; and chemical methods, which are usually designed to aid or abet weathering processes. There are, naturally, exceptions to these rules, and each remediation technique has its own window-of-opportunity for use.

Physical remediation methods include source controls, booms, skimmers, and sorbents [13]. All physical methods are dependent on weather, and most require extensive equipment to be brought to site - resulting in significant deployment lag [13]. Source controls aim to reduce the size of a spill by preventing further leakage/spillage [13]. Booms are floating barriers designed to impede oil movement. They have many different designs, and are used to prevent spreading, protect sensitive areas, or divert and concentrate oil for further remediation [6]. Skimmers are devices which collect oil from the water surface, preferably with as little accompanying water as possible. Skimmers work best on thicker slicks [6], and their use is limited by oil storage capacity. Sorbents are materials, often incorporated into a boom or mat, which absorb oil. They are particularly useful for small spills, or as a backup for other remediation methods [6].

Chemical remediation techniques used in offshore environments include in-situ burning and application of spill treating agents such as dispersants, demulsifiers and emulsion inhibitors, herders, recovery agents, biodegradation agents, non-sorbent solidifiers, and gelling agents [13, 19]. In-situ burning is fairly self-explanatory; a slick is converted to a gaseous form through burning. To be combustible, a slick must be at least 3 mm thick [20]. Dispersants are designed to remove oil from the water surface by enhancing natural processes [19]. There is, however, literature suggesting that these chemicals may inhibit biodegradation of oil [21].

Emulsion inhibitors and demulsifiers respectively prevent formation of and separate oil-water emulsions into their constituent parts, greatly reducing the volume of an emulsified slick [19]. Herders are surface-active materials that spread across the water surface, forming a contracting molecular “boom”. These chemicals interact with a spill, causing it to decrease in surface area and thicken [19, 20]. While herders only perform well in calm conditions, they show great promise for remediation amidst loose pack ice in preparation for in-situ burning [20]. Recovery agents interact with oil to facilitate removal by skimmer [19]. Biodegradation agents are typically either nutrients or bacteria, applied with the hope of increasing biodegradation rate. This comes with risk of eutrophication and competition with

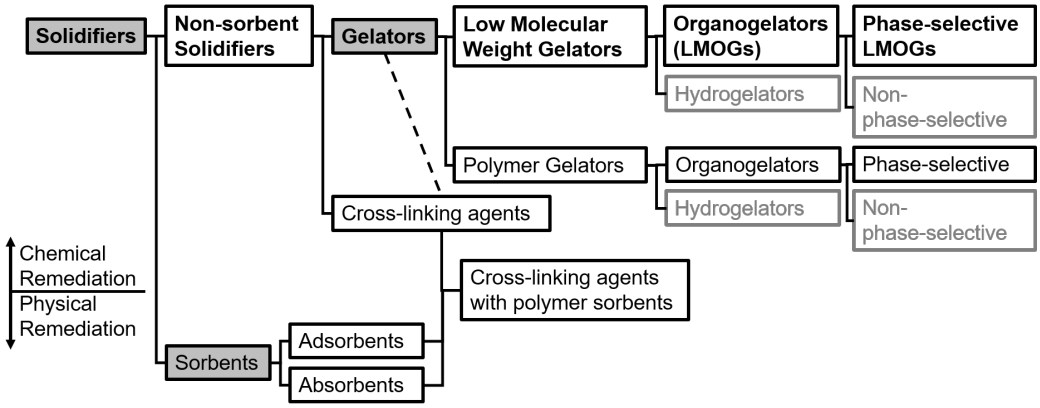

Figure 1.1: A hierarchical classification strategy for solidifiers, sorbents, and gellants (major categories shaded). While sorbents are considered a class of solidifier they are typically classified as a physical remediation strategy. Discovery of phase-selective LMOGs (bolded path) has lead to renewed interest in solidifiers as a remediation strategy. Dimmed boxes have no use in oil remediation. Modified from Figure 1 in [23].

existing species, and tests have not been promising for their utility [19]. Gelling agents and other solidifiers are designed to make a spill more solid [19], and are the technique of primary interest for this study.

Canadian federal approval of chemical spill treating agents is pursuant to the Canada Oil and Gas Operations Act based on principles of net environmental benefit. Currently, only two chemicals are approved for use: Corexit® EC9500A and Corexit® EC9580A, both of which are dispersants. Addition of other agents is the responsibility of the Minister of the Environment [22].

1.2.1 Solidifying oil as a spill response strategy

The idea to make oil spills more solid is not a new one. Indeed, development of solidifiers began in the 1960s [13, 23]. Unfortunately, the lack of standard terminology makes browsing classic references difficult. Indeed, the relationship between solidifiers, sorbents, and gellants has been the subject of considerable debate. Sorbents, after all, result in the oil being incorporated into a solid matrix. To limit discussion of this topic, we will use the classification scheme proposed by Motta, Stoyanov, and Soares [23] (Figure 1.1). The discussion here concerns itself with non-sorbent solidifiers.

Rendering of oil into an inert, continuous mat has a number of potential benefits including a reduction in spreading, preventing the formation of emulsions, and easier collection [13, 23]. These chemicals could potentially render a spill "weatherproof", increasing the window-of-opportunity available for remediation [13].

Use of gellants has been limited in North America, and documentation is both scant and not peer-reviewed [19]. The low historical use of solidifiers and gellants is due to the impractical quantities of chemical required to treat a spill [19], but there has recently been a resurgence in interest with the discovery of phase-selective Low Molecular weight OrganoGelators (LMOGs) [23]. These chemicals would require doses considerably less than that required for traditional non-sorbent solidifiers, and additionally offer opportunity for the recovery of both gellant and oil [13].

1.3 Thesis motivation and objectives

This research was inspired by ongoing work taking place at BC Research Inc. (BCRI). While there is wide variation in spill treating technologies, many become less effective with response lag. This is why the scientists and engineers at BCRI have been developing new, rapid-response chemicals to increase the window-of-opportunity available for spill treatment: herders and gellants. To aid in this broader project, titled "The Development of Hybrid Rapid Response Agents to Mitigate the Impact of Oil Spills in Marine Environments," BCRI has collaborated with several research groups at the University of British Columbia (UBC) through co-funding grants from the non-profit group Mitacs. These research groups span several departments, ranging from chemistry to civil engineering.

While other researchers are actively pursuing such topics as gellant production, application, and gelling efficiency, this thesis aims to help bridge the research gap related to the behaviour of gelled oil in real-world environments. As of writing, there is no published literature related to the behaviour of gels in linear gravity waves. The only existing paper discussing gel-wave interactions involved small-scale experiments with high-frequency waves (capillary waves) on an oscillating plate [24]. For gellants to be used successfully in spill remediation, decision makers and industry require much more information on how these materials interact with the world around them. This subject is ripe for exploration, into which this thesis aims to blaze a trail.

Existing as it does at an intersection between the disciplines of hydraulics and materials science, this work must encompass a breadth of knowledge not typically required for experts of any one constituent field. To address this while providing brand new knowledge to a budding field of research, the objectives of this thesis are to:

- Provide adequate background for the reader to understand, at least superficially, the nature of both gels and waves;
- Develop theory on the interactions between marine surface gels and wave-induced velocity gradients specifically related to strain and breakage;
- Test author-derived analytical models using a novel experimental method; and
- Establish the presence of a threshold condition causing breakage of the gel.

1.4 Thesis outline

This thesis is separated into six chapters, each of which builds upon the others in understanding the interactions between gels and waves; specifically, how the spatially variable velocities associated with linear waves can cause stretching and breakage of marine surface gels. This, the first chapter, has been focused on introducing the reader to the topic of spill response, particularly when related to gellants, and provide some expectation as to the topics explored in the remainder of this document. Chapter 2: *On the nature of gels* provides the reader with background into the world of gels, including common models for their behaviour and how velocity gradients induced by linear waves might cause them to break. Chapter 3: *Gels in waves: new theoretical developments* dives deeper into understanding gel-wave interactions, developing a simple analytical model for connecting gel strain to a linear, monochromatic wave field. Chapter 4: *Experimental design* outlines how experiments at UBC were devised to test the behaviour and breakage of gels in a wave-induced spatial velocity gradient, and Chapter 5: *Results and discussion* follows up with what happened in the experiments and notes how these findings may relate to natural wave fields. Finally, Chapter 6: *Conclusions* provides a summary of findings discovered over the course of research, and outlines potential avenues for future investigation.

Chapter 2

On the nature of Gels

What does one think of when one hears the word "gel"? Perhaps the image which comes to mind is the fluid goo one puts in their hair. On the other hand, perhaps the image is that of a self-supporting jiggly dessert sitting on a plate. The broad variety of colloquial uses for the term "gel" only adds to the confusion presented by the lack of a rigorous scientific definition for this class of substances. This leads to gel's unfortunately frequent classification in "you'll know it when you see it" substances with vague definitions, where there are diverse opinions on what really constitutes a gel [25]. This has caused significant issue and delay in this study, as will be discussed later. Loosely speaking, a gel is often defined as a soft material formed of two components: a liquid, taking up the majority the volume, and a supporting network lending structural integrity [26], a classification which excludes so-called "aerogels" which feature a gas instead of a liquid. The material forming the supporting network is called the "gellant" or "gelator". Regardless of definition, gels behave in a manner neither quite solid nor quite liquid.

Gel-like viscoelastic materials falling in this transition zone between solid- and liquid- behaviour can be split into two subcategories: "true gels" and "structured liquids". A true gel has a storage modulus (G', see below) "significantly greater" than its loss modulus (G"), ie. solid-like behaviour far outstrips liquid-like behaviour, independent of time within a reasonable range. A structured liquid, on the other hand, has G' only "slightly greater" than G" and may be mildly frequency-dependent [25]. What constitutes "significantly" compared to "slightly" is, of course, a matter of opinion, but a common cut-off appears to be if the material in question is self-supporting [27] — meaning that what constitutes a gel also depends on such factors as local gravity and timescale of interest [25]. This definition is what gives rise to the simple and popular "inversion test" to distinguish a gel from a solvent-gelator solution (sol), whereby a vial containing the material is inverted [26]. If the substance sticks to the top or falls to the bottom as a single piece, it's considered a gel; otherwise, it's a liquid.

Gels may also be defined in relation to their molecular structure. Some of these categories include polymer, metal-organic, dynamic covalent, inorganic,

and supramolecular gels [26]. This last class, supramolecular gels, has sparked recent interest in fields ranging from tissue engineering to nanotechnology to environmental remediation. These gels exhibit a number of useful and interesting properties, including response to external stimuli such as heat, light, sound, pH, and mechanical stress [26, 28]. These stimuli trigger one of a range of responses, ranging from gel strengthening/weakening to gel-sol transitions [28]. In these gels, small gellant particles form into micrometer scale fibers which entangle to form extensive lattice structures. The primary forces at play are non-covalent, including electrostatic interactions, coordinative bonding, hydrogen bonding, π-π stacking, and van der Waals forcing [28]. The most useful property for remediation, however, is that held by Low Molecular-weight OrganoGelators (LMOGs), a subclass of supramolecular gellant able to reversibly gel organic chemicals (such as oil) preferentially to water [28, 29].

2.1 Wave-gel interactions

There is only very limited research into the interactions between gels and waves [23]. What little is available in the public domain consists of a single research paper on how capillary waves could cause gel breakage [24]. Capillary waves are short ($L_w < 1.7$ cm), small amplitude waves dominated by surface-tension effects [30, 31]. To broaden the available literature as much as possible, let us here examine how a longer, linear wave might interact with a surficial gel. Linear waves are long, small amplitude sinusoidal waves [32]. An example of a deep-water linear wave is illustrated in Figure 2.1.

How could a linear wave cause a gel to break? The first mechanism which comes to mind is bending. The bending of elastic sheets on wave fields is explored in literature on floating structures [33]. While bending may lead to gel breakage, this study examines one of the other wave-induced effects.

Water particles in a linear wave move in orbits, as shown in Figure 2.1a. A water particle at the wave crest moves in the same direction as the wave, and will move the opposite direction in a wave trough. As linear waves have relatively small amplitude, this horizontal gradient may be approximated using the horizontal (x) component of particle velocity, as illustrated in Figure 2.1b. For a gel on the water surface, this means that there will be a variation in both the magnitude and direction of drag on the gel bottom. This variation in drag will exert a tensile force, causing the gel to stretch and compress linearly as each wave passes. This

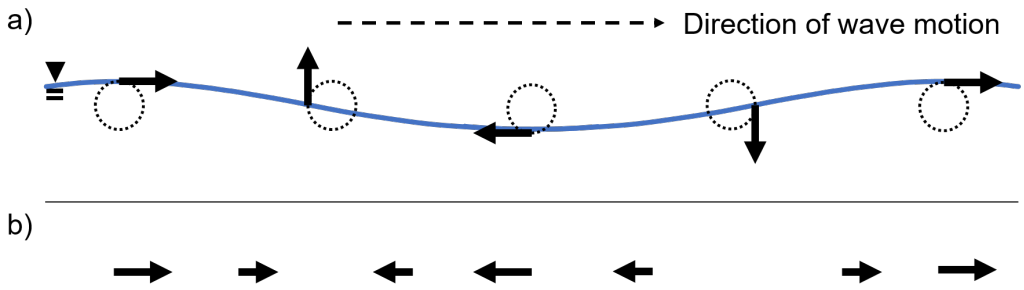

Figure 2.1: An illustration of a deep-water linear wave over approximately one wave length, where the wave is moving from left to right. (a) shows instantaneous velocity of water particles at the water surface using arrows. Particle trajectories, neglecting Stokes' drift, are indicated as dotted circles. (b) shows spatial variation in the x-component of particle velocity which, for a small-amplitude wave, is approximately equal to the velocity component parallel to the water surface. Not to scale.

periodic strain could result in gel breakage. Figure 2.2 provides a definition sketch for strain, approximated in a purely horizontal manner.

2.2 Models of gel behavior

The study of rheology addresses the characterization of gels and other materials that are neither fully solid nor fully liquid [34], known as "viscoelastic" materials. Any introduction to rheological materials will include two key models: that of an elastic solid, and that of a viscous fluid. These models relate the stress applied to a material to the associated strain. In an elastic solid, stress (σ) and strain (ε) are proportional, where the Young's Modulus (E) of the material is the constant of proportionality:

$$\sigma_s = E\varepsilon_s \tag{2.1}$$

This type of behavior may be denoted using a spring element (subscript s). The various material elements discussed here are illustrated in Figure 2.3. In a viscous liquid, stress is proportional to the time-derivative of strain, by way of the fluid's viscosity (μ):

$$\sigma_d = \mu \frac{d\varepsilon_d}{dt} \tag{2.2}$$

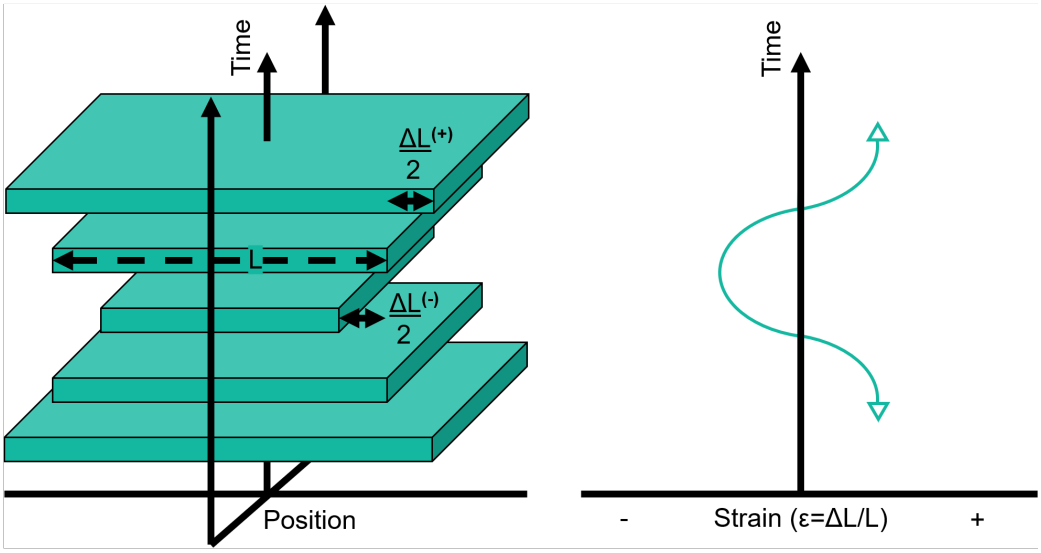

Figure 2.2: Horizontal oscillatory strain of a free object. In a marine surface gel, this will be caused by spatially variable shear stresses at the gel-water interface.

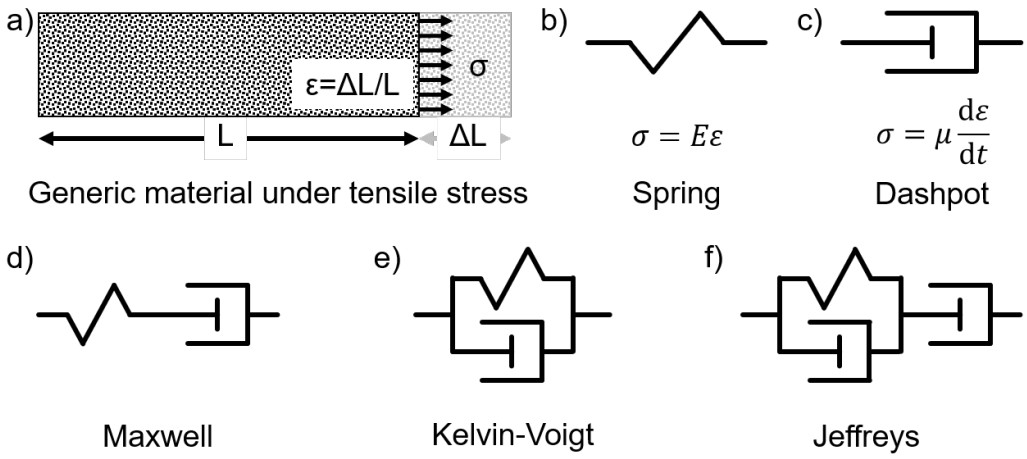

Figure 2.3: Various material elements with associated symbols and configurations. These symbols are standard in literature.

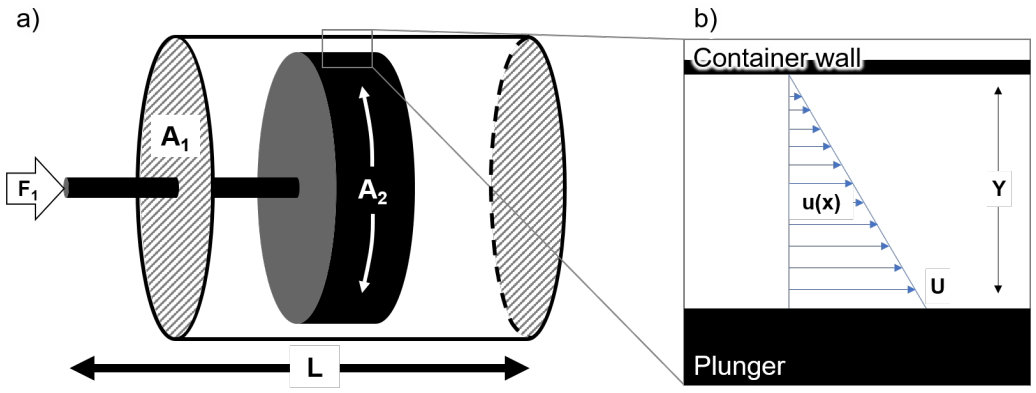

Figure 2.4: Construction of a physical dashpot (a). Movement of the plunger induces a velocity gradient between the plunger and container wall, which may be expressed as a shear stress as illustrated in (b).

This may be represented using a dashpot element (subscript d). This definition of viscosity may be unfamiliar to those coming to this study from a background of fluid mechanics, and sources make no attempt at reconciliation [35]. For the comfort of fluid dynamicists, consider the construction of a physical dashpot of the sort used in real-world damping systems. Dashpots are constructed by putting a piston in a viscous fluid; as the piston is displaced, fluid is forced to flow around it. In this manner, we transfer fluid motion to a linear "viscous" damping. This is illustrated in Figure 2.4 and further derived in the appendices.

Gels, as rheological materials, behave as neither elastic solids nor viscous liquids; but are rather a mix between the two. The two most common ways of describing viscoelastic materials are the Maxwell and Kelvin-Voigt models. A Maxwell fluid describes a material element as a spring and a dashpot element in series. As such, the two sub-elements will experience the same stress, but not the same strain. This is explored in [35].

$$\sigma = \sigma_s = \sigma_d \tag{2.3}$$

$$\varepsilon = \varepsilon_s + \varepsilon_d \tag{2.4}$$

Applying Equations 2.1 and 2.2 to the time derivative of 2.4 one may derive the following equation for Maxwell-type behaviour:

$$\frac{d\varepsilon}{dt} = \frac{1}{E}\frac{d\sigma}{dt} + \frac{1}{\mu}\sigma \tag{2.5}$$

Which, rearranged, may be presented as

$$\mu \frac{d\varepsilon}{dt} = \lambda_1 \frac{d\sigma}{dt} + \sigma \tag{2.6}$$

In the recasting of this equation we can define the material's relaxation time, $\lambda_1 = \mu/E$. This scale represents the amount of time required for internal stresses to dissipate after an applied stress is released [35]. It should be noted that a Maxwell fluid is not a true gel, as it will flow. The second common way to describe a viscoelastic material is to use a Kelvin-Voigt element, which consists of a spring and a dashpot element in parallel. In this manner, the two sub-elements will experience the same strain, but not the same stress. This is also explored in [35].

$$\sigma = \sigma_s + \sigma_d \tag{2.7}$$

$$\varepsilon = \varepsilon_s = \varepsilon_d \tag{2.8}$$

Similarly to the derivation for the Maxwell element, applying Equations 2.1 and 2.2 to 2.7 one may derive the following equation for Kelvin-Voigt-type behaviour:

$$\mu \frac{d\varepsilon}{dt} + E\varepsilon = \sigma \tag{2.9}$$

Dividing by Young's modulus,

$$\lambda_2 \frac{d\varepsilon}{dt} + \varepsilon = \frac{\sigma}{E} \tag{2.10}$$

Notice that, in recasting, another time scale becomes visible: retardation time, equivalently derived as $\lambda_2 = \mu/E$. While the derivation is the same as for relaxation, the scale here represents a delay in the elastic response as abrupt changes in stress are offloaded from the viscous element [35]. Subscripts are standard when discussing these concepts. Now, how would we expect these models to behave under an applied load? Let us consider a test where we have a constant stress $\sigma_{const.}$applied from t = 0 to t_{hold}, where the sample is held at a constant strain. After some amount of time, stress is released at t_{rel} and the experiment is allowed to proceed until t_{end}. Behavioural patterns are illustrated in Figure 2.5.

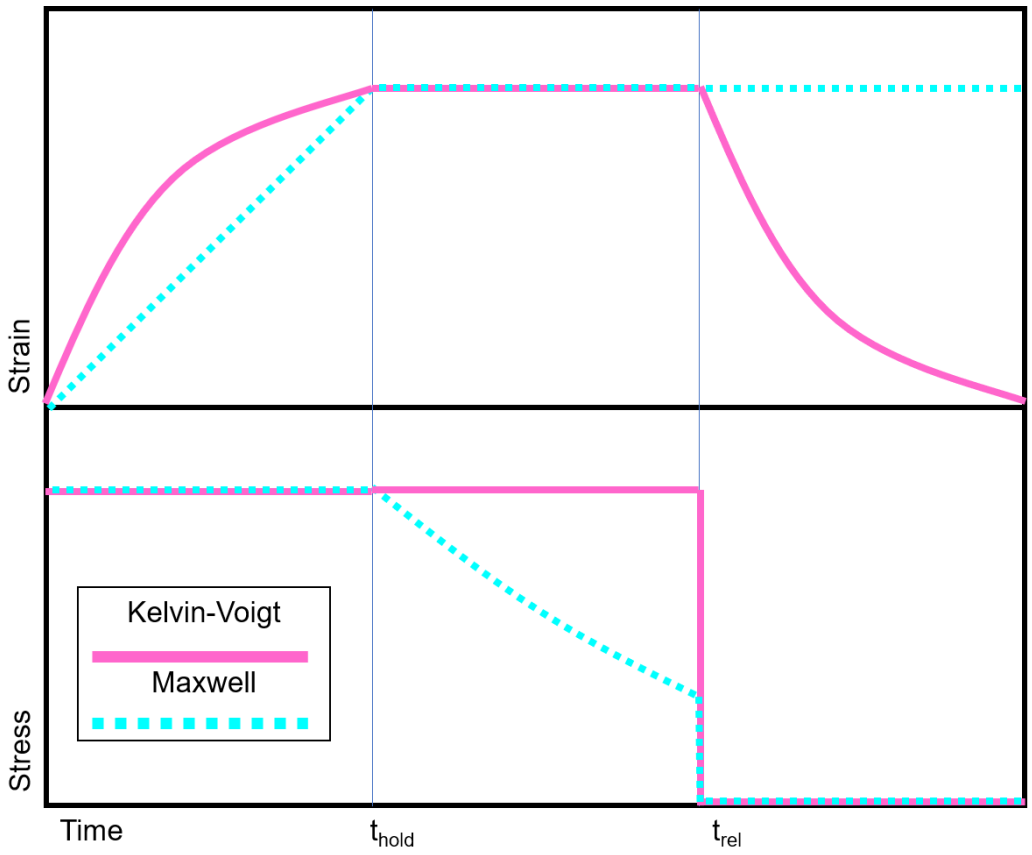

Figure 2.5: Response of viscoelastic gel models to a simple stress-strain test. A constant stress is applied from $t = 0$ to t_{hold}. The gel is held at constant strain until t_{rel}, then released.

Prior to release of the applied stress, our element will behave as follows, as derived by the author:

$$\text{Maxwell} : \varepsilon = \frac{\sigma_{const}}{\mu} t \tag{2.11}$$

$$\text{Kelvin} - \text{Voigt} : \varepsilon = \frac{\sigma_{const}}{E} \left(1 - e^{-t/\lambda_2}\right) \tag{2.12}$$

Note that the sample is initially at rest with zero strain. During the time strain is held constant:

$$\text{Maxwell} : \sigma = \sigma_{rel} e^{(t_{rel}-t)/\lambda_1} \tag{2.13}$$

$$\text{Kelvin} - \text{Voigt} : \sigma = E\varepsilon_{rel} \tag{2.14}$$

After any remaining applied stress is released, the response becomes:

$$\text{Maxwell} : \varepsilon = \varepsilon_{rel} \tag{2.15}$$

$$\text{Kelvin} - \text{Voigt} : \varepsilon = \varepsilon_{rel} e^{-(t-t_{rel})/\lambda_2} \tag{2.16}$$

Now, as this is particularly pertinent to wave response, let us consider the author-derived response of these models to sinusoidal stress $\sigma = \sigma_{max} \sin(-\omega t)$, where the gel is initially unstretched and at rest.

$$\text{Maxwell} : \varepsilon = \frac{\sigma_{max}}{\mu\omega} \left(\cos(\omega t) + \lambda_1 \omega \sin(\omega t) - 1\right) \tag{2.17}$$

$$\text{Kelvin} - \text{Voigt} : \varepsilon = \frac{\sigma_{max} \left(\lambda_2 \omega \cos(\omega t) - \sin(\omega t) - \lambda_2 \omega e^{-\frac{t}{\lambda_2}}\right)}{E\left(\lambda_2^2 \omega^2 + 1\right)} \tag{2.18}$$

2.2.1 Gels in shear-space

Most common rheological testing takes place under shear, likely because tensile tests are difficult to conduct with a flowing material. As such, shear-tests provide shear moduli instead of Young's moduli. Consider an oscillatory shear experiment, where a material is subjected to a sinusoidal strain. This is similar to the situation explored in 2.17 and 2.18, but from a shear stress perspective instead of linear strain. Let us consider shear stress (τ) to be the product of the shear strain (γ) and complex shear modulus (G^*). For a rheological material, some portion of the stress will be related to the shear strain (as in an elastic solid) and some

portion will be related to shear stress (as in a viscous liquid). As the applied strain is sinusoidal, so will be the applied stress. As such, we may present stress as

$$\frac{\tau}{\gamma} = G^* = G' + iG" \tag{2.19}$$

where the storage modulus (*G'*) is representative of elastic behaviour and the loss modulus (*G"*) is representative of viscous behaviour. We could also, instead, write this using a phase angle (δ), which represents the delay of stress response from an applied sinusoidal strain

$$G^* = \frac{\tau}{\gamma}\cos\delta + i\frac{\tau}{\gamma}\sin\delta \tag{2.20}$$

The tangent of the phase angle is also termed the "loss factor" [36]. The complex shear modulus is related to the complex Young's modulus (*E**) by way of $E^* = 2G^*(1+\nu_{Poisson})$. In an incompressible material $\nu_{Poisson} = 0.5$, which allows us to write the simple relationship $E^* = 3G^*$ [36]. The final step is to convert Young's storage and loss moduli back to a Young's modulus and viscous parameter. This translation will be different for different gel models. First, consider the Kelvin-Voigt response to the signal $\varepsilon = \varepsilon_{max}\Re\left(e^{i\omega t}\right)$. Comparing the stress response written in terms of both E^* and E:

$$E' + iE" = E + i\mu\omega \tag{2.21}$$

therefore

$$E = 3G' \tag{2.22}$$

$$\mu = 3G"/\omega \tag{2.23}$$

Now consider a Maxwell response to the signal $\sigma = \sigma_{max}\Re\left(e^{i\omega t}\right)$. Comparing the strain response written in terms of both E^* and E:

$$E' + iE" = \frac{iE\mu\omega}{E + i\mu\omega} \tag{2.24}$$

where the only viable solution is, knowing all constants are real and non-zero,

$$E = \frac{3(G'^2 + G"^2)}{G'} \tag{2.25}$$

$$\mu = \frac{3(G'^2 + G"^2)}{\omega G"} \tag{2.26}$$

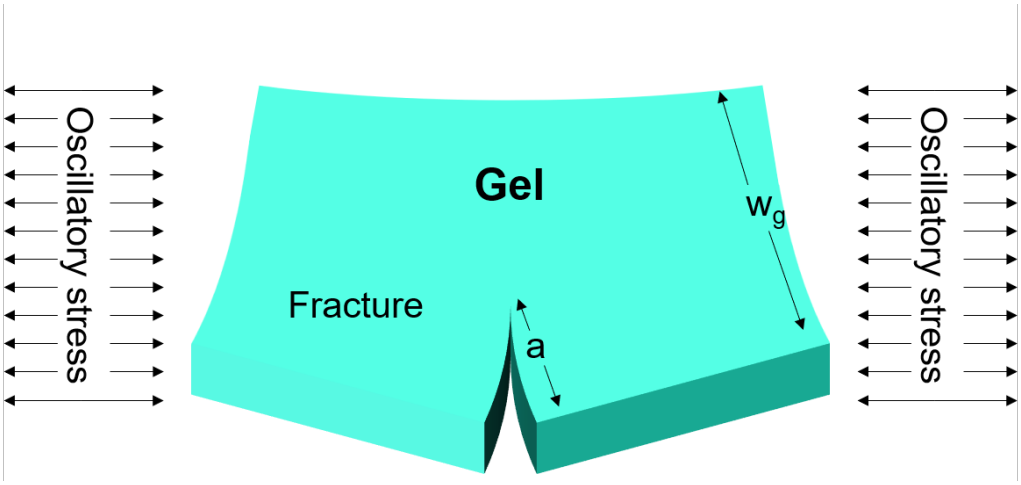

Figure 2.6: Definition sketch of a Mode I (opening) fracture under an oscillatory stress. Other categories of fracture include Mode II (sliding) and Mode III (tearing). In the case of this study, oscillatory stress is caused by differential shear across the surface of the gel.

2.3 Models for gel breakage

Any material will fail under sufficient stress. What classifies as "sufficient stress" and, indeed, what constitutes "failure" is, however, often much less clear. In the case of this study, we are interested in what conditions will lead to the Mode I (opening) fracture of a gel under an oscillatory stress acting along the plane of the gel, illustrated in Figure 2.6. Two common causes for breakage include yielding, which involves supplying sufficient force to permanently deform a material, and fatigue failure, whereby a crack extends through a material by repeated loading.

2.3.1 Yield Stress

By far the most quoted threshold for failure is the so-called "yield stress". In a rheological material, the yield stress is taken to be the stress threshold below which a material behaves elastically, and above which a material will flow [37]. Unfortunately, while it is often quoted as a singular number, a given material may be assigned completely different yield stress values depending on testing and handling techniques. Indeed, for time-dependent materials the concept becomes so ill-defined that one may only quote an "apparent" yield stress [37]. Let us

examine two yield-stress measurement approaches: stress ramp and oscillatory strain sweep. Figure 2.7 illustrates how yield stress may be determined using these techniques.

Figure 2.7a illustrates the concepts of "static" and "dynamic" yield stresses using a stress-ramp experiment. The static yield stress represents the stress required to initiate flow of a viscoelastic material; dynamic yield stress represents the stress to arrest flow [37]. This is similar in concept to the coefficients of static and kinetic friction. In a stress ramp experiment, stress is increased from zero until a point above which the material has started to flow. Stress should then be decreased to back to zero. Strain rate will abruptly start to increase at the static yield stress during the up-ramp, and will decrease to the dynamic yield stress during the down-ramp [37].

Oscillatory measurements of yield stress are obtained from an oscillatory strain sweep experiment at a selected frequency. The results of such an experiment are shown in Figure 2.7b. This type of analysis has the distinct advantage of being associated with a frequency, which may be matched with a given wave-field. There are several methods to determine yield stress from an oscillatory strain sweep, and there is debate over which technique is "correct". The most common method identifies yield stress as the stress associated with the intersection between "sufficiently" early-data and late-data fit lines on a plot of elastic modulus against stress [37]. This is illustrated in Figure 2.7b. The second, and much less subjective, approach is to use the peak elastic stress, which is the product of the storage modulus and strain [39]. This method is shown in Figure 2.7c. As waves will subject a gel to oscillatory conditions, measurements of oscillatory yield stress are likely to be more reflective of results than static or dynamic measurements. This study makes use of the elastic stress method to determine yield stress.

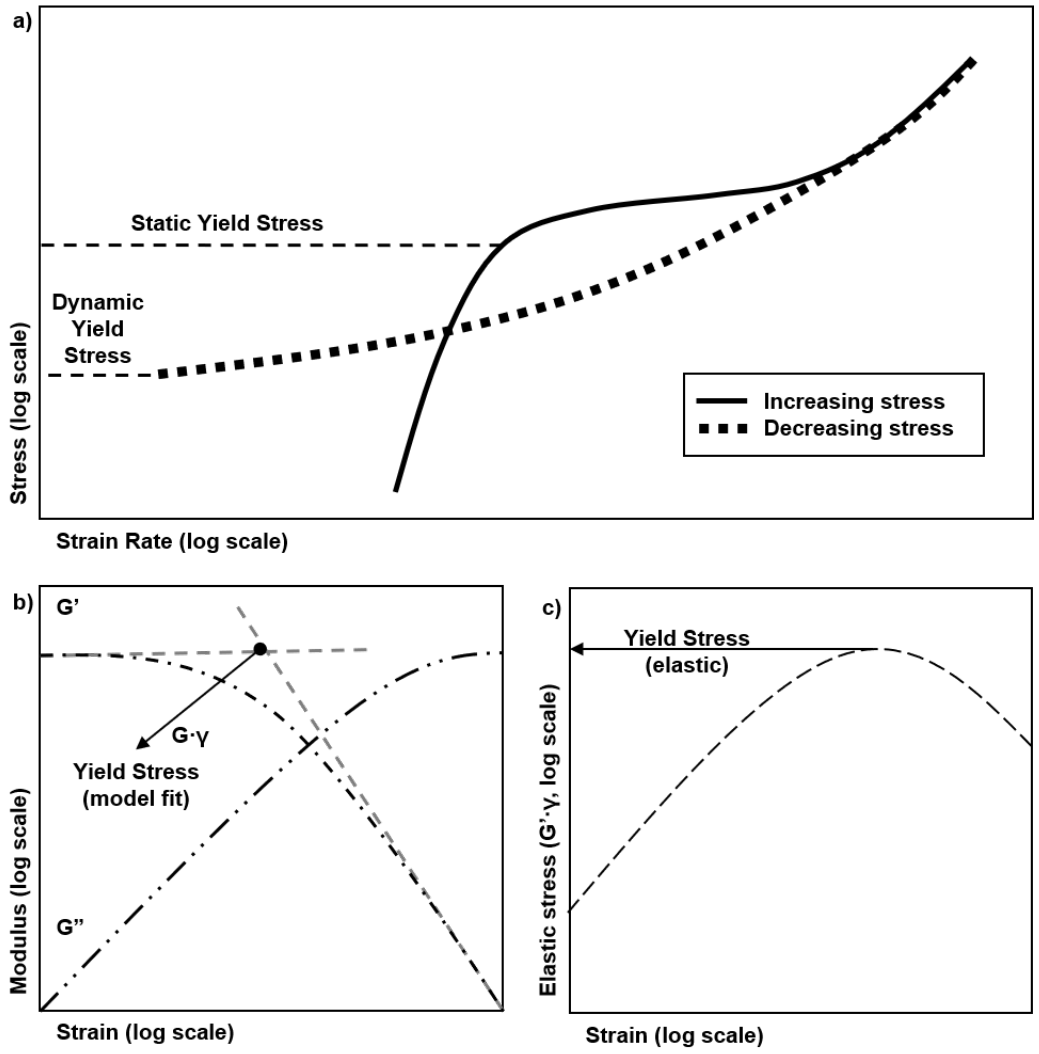

Figure 2.7: Analysis techniques for determining yield stress in rheological materials. (a) Results of a stress-ramp experiment illustrating static and dynamic yield stress. (b) Results of an oscillatory shear experiment illustrating a typical method of determining the yield stress. (c) Results of an oscillatory shear experiment illustrating how to determine the yield stress using the elastic modulus. All methods find use in various sources. (a) based on [38], (b) on [37], and (c) on [39].

Chapter 3

Gels in waves: new theoretical developments

Differential shear stresses along the length of a marine surface gel will result in stretching. These shear stresses will be induced by the boundary layer next to the gel, where water particles are moving parallel to the gel plane. In the case of a linear wave, where $H \ll L_w$, water particle velocity parallel to the gel surface may be approximated as the horizontal component of particle velocity.

3.1 The wave boundary layer: Stokes' second solution

Wave boundary layers are complex phenomena. As such, we use simplified models to describe what happens at an interface between an oscillating fluid (such as our wave) and a surface (such as a gel). One such simplified model is that of Stokes' Second Problem, where an flat, infinite plate is oscillated in an infinite fluid. This problem is outlined in more detail in classic boundary-layer texts [40].

It is not difficult to recast this as an oscillating fluid instead of an oscillating plate. Consider the solution, following [41], where the fluid oscillates as $u_\infty = U_\infty \cos(-\omega t)$ at a distance sufficiently far from the plate. The laminar velocity field at the plate boundary, using values applicable in experimentation, is illustrated in Figure 3.1. The associated stress is shown in Equation 3.1, where $\Re$ denotes the real component and $i$is the imaginary unit.

$$\tau = \Re\left[\rho_w \nu_w U_\infty \sqrt{\omega/2\nu_w}(1+i)e^{i(\omega t)}\right] \tag{3.1}$$

Or, if we introduce a term for peak shear stress $\tau_{max} = U_\infty \rho_w \sqrt{\omega \nu_w}$, the trigonometric solution becomes

$$\tau = \tau_{max} \cos(-\omega t - 3\pi/4) \tag{3.2}$$

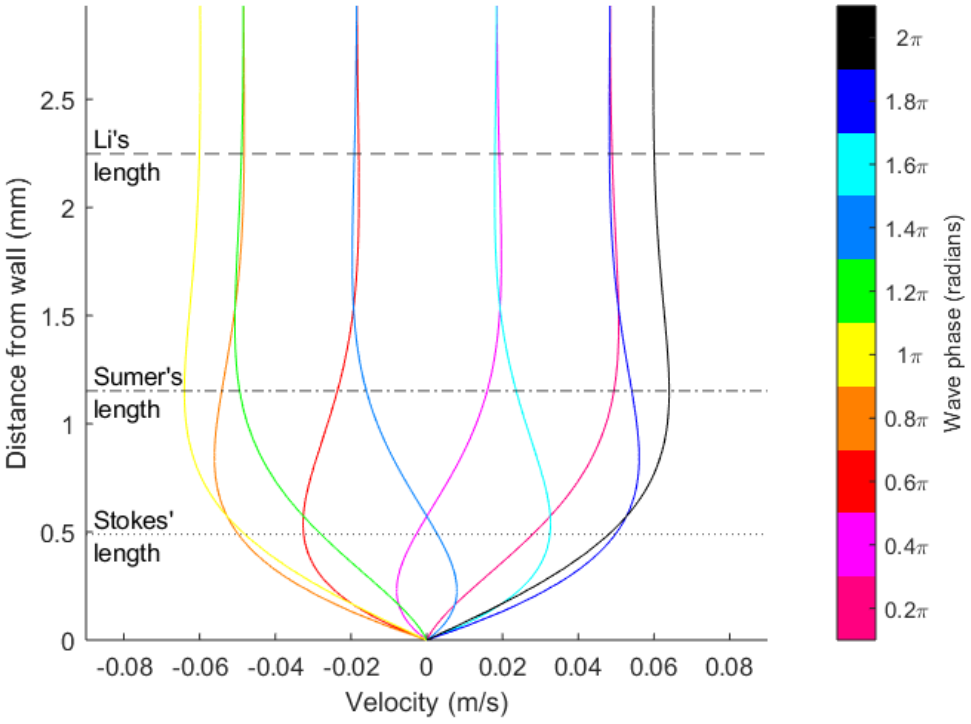

Figure 3.1: Solution to Stokes' second problem, modified for oscillating current and presenting three boundary layer estimates. Stokes' length ($\delta_{Stokes} = \sqrt{\nu T/\pi}$) is a simple viscosity-period relationship, ideal for oscillating-wall problems. Sumer's length represents the location of maximum velocity ($\delta_{Sumer} = \frac{3\pi}{4}\delta_{Stokes}$). Li's length ($\delta_{Li} \approx 4.6\delta_{Stokes}$) falls where velocities come within 1% of free stream velocity for the whole wave period [42, 43]. Parameters are within the range used in experimentation ($U_\infty = 0.06$ m/s, $T = 0.75$ s). Li's length was less than 2.5 mm in all experiments. This becomes important when considering wall effects in experimental analysis.

Now what remains is to apply this solution to a gel. We will select U_∞ as the peak value at the gel surface as predicted by linear wave theory. Unlike in Stokes' problem, a wave field has both spatial and temporal periodicity. Assuming that Equation 3.2 applies locally in space, the wave field described by

$$u = U\cos(kx - \omega t) \tag{3.3}$$

adjacent to a gel will produce a stress field

$$\tau = \tau_{max}\cos(kx - \omega t - 3\pi/4) \tag{3.4}$$

This stress field may be assumed for any case where the plate velocity is sufficiently less than U.

3.2 Forces in a gel due to wave stress

The shear force exerted on the gel (3.4) can be interpreted in two ways: the net force, causing advection, and the differential force, which will lead to stretching. Consider a finite, rectangular plate exposed on one side to a variable horizontal velocity gradient as in Figure 2.1b or Equation 3.3. Neglecting edge effects, assume that the stress-field solution 3.4 holds everywhere on the plate. Plate length L_g is in the direction of wave motion and plate width w_g is orthogonal to the wave. Plate depth d_g is only used to express tensile forces as stresses, and is otherwise neglected.

3.2.1 Forces governing advection

Net force on our plate may be calculated with a simple integral. Written as a function of location of the center of mass on our plate (x_g),

$$F_{drift} = w_g \int_{x_g - L_g/2}^{x_g + L_g/2} \tau \mathrm{d}x = 2\frac{\tau_{max} w_g}{k}\sin\left(\frac{kL_g}{2}\right)\cos(kx_g - \omega t - 3\pi/4) \tag{3.5}$$

If variation in plate length is sufficiently small, only the cosine term in Equation 3.5 is variable.

Any movement of the plate will cause stress to deviate from a simple sinusoidal signal; however, if advection is sufficiently small it may be neglected in

analysis of stretching. Consider a low-drift scenario. In such a scenario, the kx_g term may be neglected if the plate is centred on the origin. In this case, for an initially stationary plate, one finds that the maximum plate velocity will be

$$u_{g,max} = \frac{2\tau_{max} w_g}{k\omega m_g} \sin\left(\frac{kL_g}{2}\right) \tag{3.6}$$

If this velocity is low compared to background water particle velocity it may be neglected in calculation of the stress field.

3.2.2 Forces governing stretching

Now let us consider the average tensile force across the sheet. The tensile force acting at a point within a sheet, where x' represents distance from the left end of the sheet, is

$$F_T = \int_{x_g - L_g/2 + x'}^{x_g + L_g/2} \tau w_g \mathrm{d}x - \int_{x_g - L_g/2}^{x_g - L_g/2 + x'} \tau w_g \mathrm{d}x \tag{3.7}$$

$$= \frac{\tau_{max} w_g}{k} \left[\sin(\alpha + L^*) + \sin(\alpha - L^*) - 2\sin\left(\alpha - L^* + kx'\right)\right] \tag{3.8}$$

Here, $\alpha = kx_g - \omega t - \frac{3\pi}{4}$ and $L^* = kL_r/2$. This means that the tensile force on the centre of the sheet ($x' = L_r/2$) is

$$F_{T,centre} = 2\frac{\tau_{max} w_g}{k} \left[\cos(L^*) - 1\right] \sin(\alpha) \tag{3.9}$$

This tensile force at the centroid is what will eventually lead to failure, as it is of the greatest amplitude compared to the rest of the plate. Net stretching of the plate, however, will be the result of average tensile force across the length of the plate. This force is governed by

$$\overline{F_T} = \frac{1}{L_g} \int_0^L F_T \mathrm{d}x' = \frac{2\tau_{max} w_g}{k} \left[\cos L^* - \frac{\sin L^*}{L^*}\right] \sin\alpha \tag{3.10}$$

3.3 Simplified Model of Gel Stretching

Assuming negligible drift, Equation 3.10 may be expressed as

$$\sigma_T = \sigma_{max} \sin(-\omega t) \tag{3.11}$$

for a gel centred at $x_g = 0$ and neglecting phase delay between wave and force. We will define σ_T as the spatial-average tensile stress experienced by the plate and σ_{max} as the peak value of σ_T. This may be applied to 2.17 and 2.18 to predict the author-derived non-inertial response of the gel to wave forcing. For a Maxwell material,

$$\varepsilon = \frac{1}{\mu\omega}\frac{2\tau_{max}}{kd_g}\left[\frac{\sin L^*}{L^*} - \cos L^*\right]\left(\sqrt{\lambda_1^2\omega^2+1}\sin(\omega t + \phi_{Ma}) - 1\right) \tag{3.12}$$

where $\phi_{Ma} = \tan^{-1}\left(\frac{1}{\lambda_1\omega}\right)$. For a Kelvin-Voigt material,

$$\varepsilon = \frac{1}{E\left(\lambda_2^2\omega^2+1\right)}\frac{2\tau_{max}}{kd_g}\left[\frac{\sin L^*}{L^*} - \cos L^*\right](\\ \sqrt{\lambda_2^2\omega^2+1}\sin(\phi_{KV} - \omega t) - \lambda_2\omega e^{-\frac{t}{\lambda_2}}\Big) \tag{3.13}$$

where $\phi_{KV} = \tan^{-1}(\lambda_2\omega)$. To visualize the difference between these models, consider the response of the following arbitrary gel subjected to forcing similar to that experienced by the experimental gel, presented in Figure 3.2.

Literature varies on which model is most applicable for gelatin, the gel used in this study. A study on bovine gelatin found a Maxwell model to work for concentrations greater than 3% by weight, with a more complex model for lower concentrations. The retardation and relaxation times for these experiments were order 1 and 10^{-6} seconds respectively [36]. Another study, this time on porcine gelatin, used a Kelvin-Voigt model with relaxation time of order 10^{-4} s for a 3% concentration gelatin [44]. The values for retardation and relaxation in the Figure 3.2 are 5.7 s and 0.0025 s as determined from shear shear storage and loss moduli.

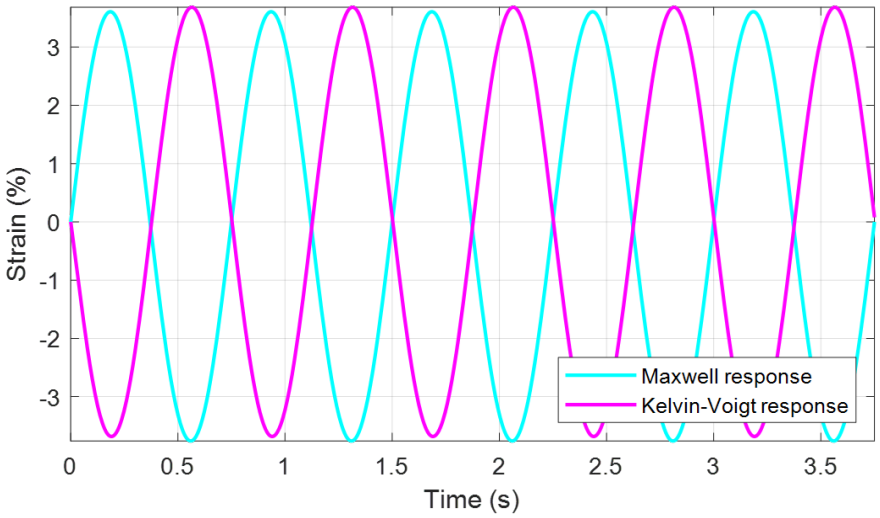

Figure 3.2: Comparison of gel models for the gel in Experiment F. Viscous parameters and Young's moduli for the Maxwell and Kelvin-Voigt responses based on G' = 28.5 Pa and G" = 0.6 Pa.

Chapter 4

Experimental design

The most directly applicable way to test the behaviour of a gel subjected to wave action is to apply waves directly to a gel in a wave tank. Two wave tanks were available for experimentation, one at UBC and one at BCRI. The two tanks, shown in Figure 4.1, vary significantly in both size and functionality.

The UBC tank is approximately 3.3 m in length, from the midpoint of the wave generator oscillation to the toe of the wave absorber, and is 21 cm in width. Water depth is controlled using an overflow weir and, as such, the tank must have a source of water available continuously. Net water flow may be avoided by putting the water source behind the wave generator, next to the weir. As the weir feeds directly into a building-wide water recirculation system this tank is not oil-safe, and great care must be taken to ensure all materials tested in the tank are recovered as much as possible. The wave generator in this tank consists of a plate which oscillates horizontally (primarily), with continuously variable thrust length and frequency. In this way it most resembles a piston-type wave generator, a style which lends itself best to shallow-water wave generation [45]. The machine must, however, be fully stopped to change thrust length. The wave absorber is a wedge-shaped beach constructed of gravel and covered by synthetic horse-hair mesh at a slope of 1:7. This is a fairly typical design for a passive wave absorber [46].

The BCRI tank is 15 cm in width and approximately 1.2 m from wave generator to the base of a plunging-style wave generator. The fine synthetic horsehair wave absorber is 40 cm long at a slope of 1:5. This tank also has the ability to run a current through the tank in the same direction as wave motion, with water recirculating from one end of the tank to the other. The advantage of this tank is that it is oil-safe.

Taking advantage of the larger tank at UBC, the author decided upon a novel experimental methodology to isolate stretching due to velocity gradients from wave-induced bending effects: bottom-of-tank experimentation. To understand the consequences of this experimental mode, consider a wave in intermediate depth, as shown in Figure 4.2.

a) University of British Columbia

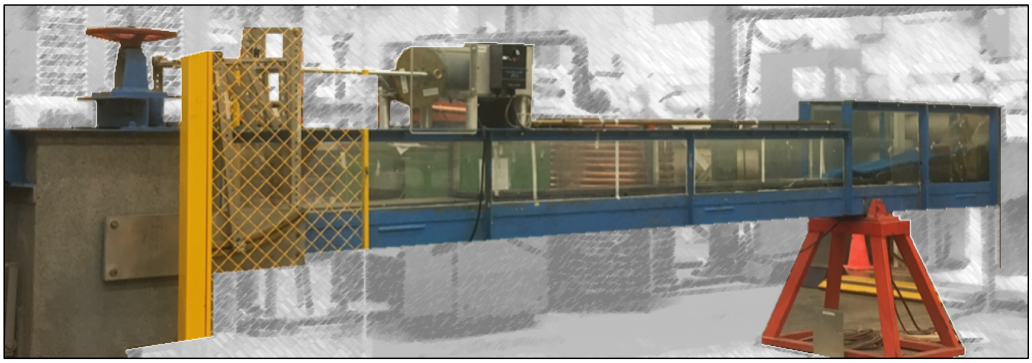

b) BC Research Inc.

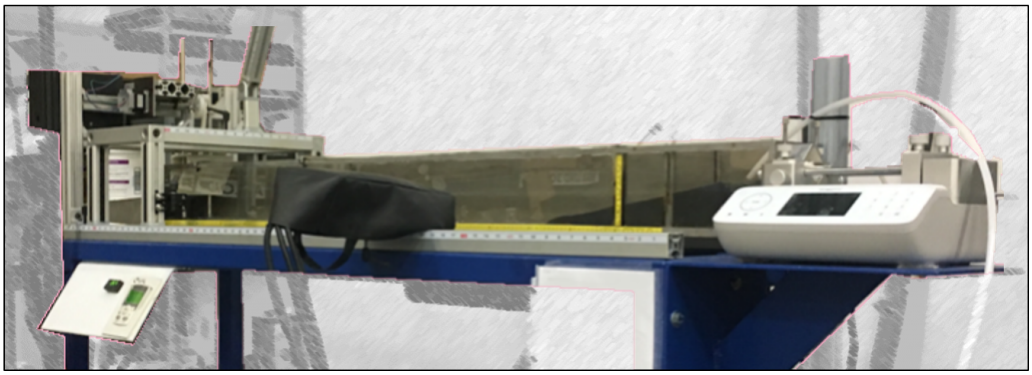

Figure 4.1: Wave tanks used in experimentation at (a) the University of British Columbia (3.3m) and (b) BC Research Inc. (1.2m). Wave generators are on the left side of each image, wave absorbers on the right. Motor and wave generator mechanism are visible in (a), but the paddle is occluded. The tank in (b) visibly features a mounted camera for Particle Image Velocimetry, syringe pump, and control panel for current and temperature. Backgrounds have been blurred for clarity.

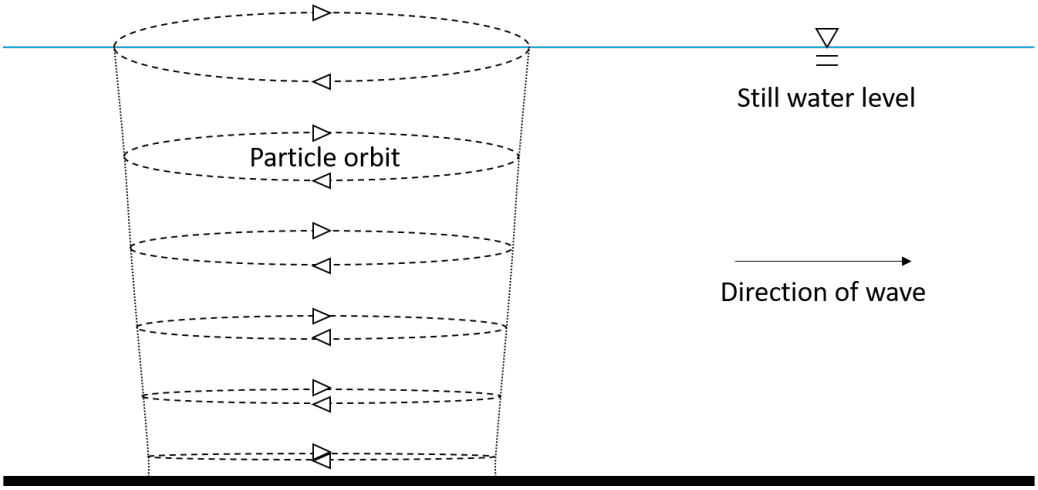

Figure 4.2: Decay of particle orbits in a linear wave of intermediate depth, neglecting Stokes' drift.

According to linear wave theory, water particles move in elliptical orbits (closed but for Stokes' drift). In deep water these ellipses become circles. These ellipses decrease in size both vertically and horizontally with depth until, at the interface with the bed, the vertical component of motion is gone. In water of shallow to intermediate depth, this leaves a horizontally oscillating velocity gradient at the bed. We may take advantage of this purely horizontal oscillatory motion to model the velocity profile underneath a surficial gel, without dealing with wave-induced bending.

Initially, the experimental regime was intended to include top-of-tank experiments using oil gels at BCRI. By comparing predicted breakage using the author-derived formulas to those seen experimentally, one could have compared the relative importance of bending and stretching effects. Sadly, only one, qualitative, preliminary top-of-tank experiment could be conducted due to laboratory closures associated with the COVID-19 pandemic. The experiment in question has been is discussed in Appendix C.

4.1 Gel selection and properties

It is most advantageous to select a dense gel for a bottom-of-tank test, as this makes it easier to keep the gel on the bottom of the tank. Fortunately, there are

a number of relatively dense, water-based gels to choose from. While it was initially thought that paper pulp, as a macro-scale fibrous network, would perform adequately as a model for a micro-scale fibrous network (the gel), the tendency for paper pulp to immediately disperse into the water column quickly eliminated it as an option. The next series of experimental attempts used Carbopol EZ-2 polymer, a commercially available polymer from a family of products frequently used in industry as thickening agents. These "carbomers" are a common gel model used in academic research. After procurement of both product and associated equipment was finally achieved, the material was found to be a structured liquid rather than a true gel and thus unusable. This being unsuccessful, and lab availability now becoming an issue, a quantity of consumer-grade commercial pork gelatin was acquired. Preliminary experimentation found this to behave, at least qualitatively, in a manner sufficiently similar to spill-treating agents currently under development to merit further investigation. After a source was found that provided sufficient bulk quantities of the material, experimentation could begin in earnest.

Gelatin is not a single chemical, but is rather a family of products with varying properties typically produced from animal sources. Gelatin is a form of partially hydrolyzed collagen. Collagen is a family of fibrous protein structures, and is the most common class of protein found in animals. "Conditioning" involves the acid or alkaline treatment of animal tissue and thermal processing resulting in a gelatin product. The most common source of gelatin globally is pig skin, followed by bovine hide splits. Pig skin gelatin requires an acidic treatment, but bovine gelatin may be processed in acidic or alkaline fashion [47]. The wide variation in gelatin sources and quality means that there is no good literature source for its properties. Its nature as a non-uniform substance also means that models for fatigue based on molecular properties are not applicable. Unfortunately, some existing studies classify gelatin as a Maxwell fluid rather than a true gel [36]. However, literature is not wholly in agreement on this topic, as Kelvin-Voigt models have also been used [44]. Regardless of model, gel properties should remain stable with scale.

4.2 Setup

As bottom-of-tank experiments could be done with a non-oil based gel, these tests were conducted in the UBC tank. A conceptual view of the test setup is presented in Figure 4.3. As the water level in this tank is weir-controlled, the tank must be continually filled throughout experimentation. This results in the rapid

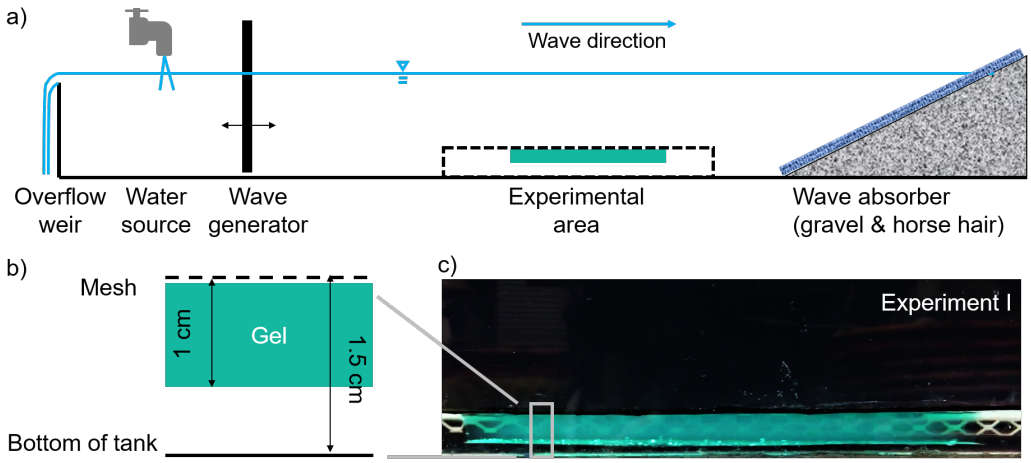

Figure 4.3: Experimental setup in the UBC tank with experimental photograph for clarity. Gel is suspended underneath the mesh due to the presence of air bubbles on the bottom of the gel, visible in the experimental photograph. Diagrams not to scale. Interpretation of photograph should account for artifacts of perspective.

accumulation of air bubbles on the bottom of any dense gel, which eventually leads to gel surfacing. To prevent gel floating and drift out of the experimental zone, a stainless steel diamond mesh was cut to provide a 60 cm long, 17 cm wide experimental section of approximately 1.5 cm in height, placed 2.1m from the average thrust of the wave generator and 0.6m from the wave absorber.

Early experimental attempts used waves that were fairly long relative to tank length, resulting in a pointed wave profile characteristic of cnoidal waves. In order to circumvent this, a new wave period was selected to keep the Ursell number ($U_r = HL_w^2/d^3$) considerably less than 26 - a requirement for linear wave theory [48]. The selected wave period of 0.75s ensured linear waves were present in experimentation ($U_r < 0.92$ in all cases). Two water depths, 12.5 cm and 15 cm, were selected to provide a range of shear stresses to the gel while maintaining a consistent wave period.

In order to both mimic the heterogeneity observed in experimental oil-gels and ensure a consistent breakage location, a 4 mm incision was made halfway along the length of each gel sheet, for the full depth of the gel and facing the camera. Due to the difficulty in making these incisions, there was often some degree of irregularity. An example of such an incision is shown in Figure 4.4.

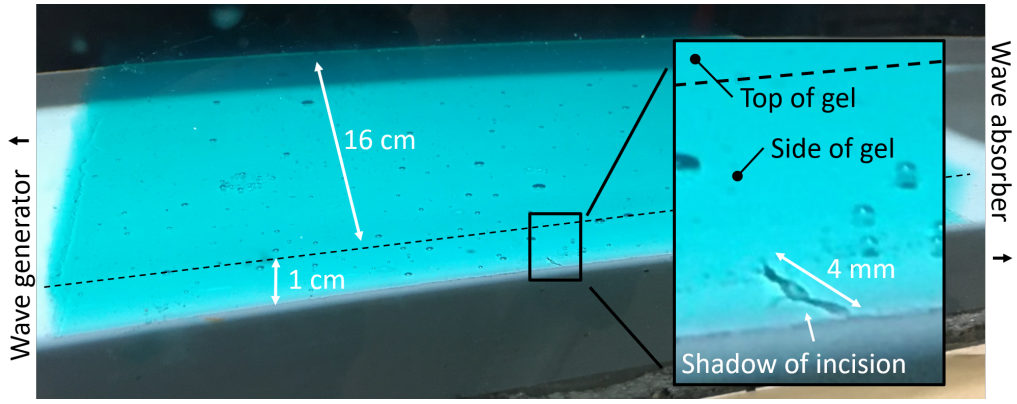

Figure 4.4: An example of a gel incision, extending 4 mm into the gel for the entire gel depth (denoted "a" in Figure 2.6). Note that the incision itself is invisible; only the shadow may be observed in the image. The dashed line indicates the corner between top and side of the gel. Bubbles are underneath the gel, and are not embedded in the gel bulk. Mesh was placed after photo was taken. This gel was used in Experiment J.

Experiments were deemed to be complete when either the gel sample had broken or a half hour (2400 wave periods) had passed with no observed breakage. Two cameras were used to capture data. The first observed the experiments from a top-down view through a mirror, and recorded each experiment in its entirety. The second was hand-held and recorded intermittently including startup and, in most cases, either breakage or late-time behaviour. Unfortunately, due to both the refraction of light by the waves and brightness of the mesh, the former recordings were left unused, in favour of the hand-held footage.

4.3 Modifying theory for bottom-of-tank experimentation

The bubble-induced buoyancy of a submerged gel in continuously renewed tap water provides a challenge in the development of theoretical models, as the oscillatory velocity field requires more consideration than a simple application of linear wave theory. For the sake of simplicity, let us assume that the gel has no impact on the overall velocity field predicted by linear wave theory, outside of boundary layer interactions. Fortunately, velocity variation is not particularly significant

with vertical change; the variation in peak velocity over the entire experimental zone is less than one percent according to linear wave theory. As such, velocity as predicted with linear wave theory for the bottom boundary will be used as U for all bottom-of-tank calculations.

While literature suggests that flow under a fixed horizontal plate is uniform in space [49, 50, 51], the small gel width and presence of gaps on either side will likely permit enough flow that this will not be the case. Taking this into account, and knowing the Li layers from gel and tank bottom are small enough to have no great interaction, we will assume that the stress experienced at the bottom face of the gel will be equivalent to that of a simple, uncovered, flat boundary. Above the gel, the mesh provides an obstruction to adjacent flow, reducing the shear stress applied to the gel. As the selected mesh was fairly substantial for structural reasons, covering approximately two-fifths of the available surface area, one can expect that less than 60% of horizontal stress predicted by linear wave theory will actually be realized in an experiment. The presence of the mesh will also generate eddies at the gel surface, as would be the case with ripples on a sand bed [52, 53]. Unfortunately, studies addressing the velocity distribution of an oscillatory boundary layer within a depression are absent from literature, so this 60% value will be used as a simple approximation. To understand the shear stress experienced by a bottom gel under a grid, let us consider what would otherwise be the shear stress on an uncovered flat boundary. By linear wave theory, the velocity immediately above the bottom boundary will be [30]:

$$u_{z=0} = U\cos(kx - \omega t) \tag{4.1}$$

where $U = \pi H/(T\sinh(kd))$. This would normally result in a stress distribution as in Equation 3.4. This gel, however, is partially obstructed by a mesh. Let us therefore assume that the gel will only experience a certain consistent fraction of the applied stress due to interactions with the mesh and exposed area on the gel sides and bottom. This will be represented by adding a coefficient to the applied stress term. The effective τ_{max} term, τ_{eff}, may be expressed as

$$\tau_{eff} = (C_O + 2d_g/w_g + 1)U\rho_w\sqrt{\omega\nu_w} \tag{4.2}$$

where C_O represents the open fraction of the mesh, and the $2d_g/w_g + 1$ term accounts for force on the sides and bottom of the gel. This will result in the following

peak spatial mean and centroid tensile stresses:

$$\sigma_{max} = \frac{2\tau_{eff}}{kd_g}\left|\cos L^* - \frac{\sin L^*}{L^*}\right| \tag{4.3}$$

$$\sigma_{mid,max} = \frac{2\tau_{eff}}{kd_g}\left[1 - \cos L^*\right] \tag{4.4}$$

To validate that the assumption of negligible drift velocity is valid for gel stretching, let us consider the velocity of the gel (Equation 3.6) relative to the water particles nearby (Equation 4.1). This ratio may be calculated according to Equation 4.5. Note that the underside of the gel is included here, as sloshing will contribute to advection.

$$\frac{u_{g,max}}{U} = \frac{2(1 + C_O + 2d_g/w_g)\rho w_g\sqrt{\nu}\sin(L^*)}{km_g\sqrt{\omega^3}} \tag{4.5}$$

For the experiments conducted in this study, this ratio ranges between six and seven percent.

Chapter 5

Results and discussion

While preliminary experiments took place over the whole of autumn 2019, the final experimental setup and gel selection were not completed until early December of that year. Lab availability constrained all testing to that month and, as such, the experimental regime took place between the 6^{th} and 17^{th} of that month. Over that course of time, twelve constrained bottom-of-tank experiments were of high enough quality to merit analysis. Varying experimental parameters are listed in the Table 5.1 and parameters held constant are listed in Table 5.2. All of the gels were observed to experience some degree of oscillatory strain, as shown in Figure 5.1.

In addition to extension and compression, gels had a tendency to drift - both oscillating within a wave and experiencing a net drift over repeated waves. Net drift was slow in all cases, and direction was unpredictable. Gels that drifted towards the beach tended to break and gels that drifted towards the generator tended to remain intact, but there were exceptions in both directions. Where gel breakage did occur, fracture extended the width of the gel in less than 1.5 minutes. Gel fracture is explored further in Figures 5.2 and 5.3.

Gel breakage was caused by crack extension. Crack length increased in each wave while the gel was in tension. This recurrent cycle resulted in a striated crack, with distance between striations increasing with distance from the initial crack location. This is shown in Figure 5.3b, where the initial incision was made on the left.

Analysis of experimental footage took place in early 2020, and is illustrated visually in Figure 5.4.

Video segments were selected and clipped to exclude both startup and breakage; the former by starting clips at least two wave periods from startup and the latter through observation. These clips were then stabilized and masked automatically. Additional processing was required to remove reflections and isolate gel location in each frame. Gel end locations were isolated frame by frame in terms of pixels, and strain calculated relative to average gel length observed during the clip. As there was some variation in peak strain throughout each experiment, a si-

Table 5.1: Parameters varied in experimentation at UBC.

Experiment		**Value (cm)**			**Featured in**
No.	**Date**	L_r	d	H	**Figure No.**
A	12/06	16	15.0	2.2	
B	12/09	14	15.0	2.4	
C	12/12	18	15.0	2.5	5.4
D	12/12	18	12.5	1.9	5.1, 5.2
E	12/13	16	12.5	1.9	
F	12/13	29	12.5	1.9	3.2
G	12/13	14.5	12.5	2.0	
H	12/16	22	12.5	1.9	
I	12/16	17	12.5	1.9	4.3
J	12/17	20	15.0	2.4	4.4
K	12/17	15	15.0	2.4	

Table 5.2: Parameters held constant in experimentation at UBC.

Description or symbol	**Value**	**Unit**	**Source**
Gravitational acceleration (g)	9.81	m/s^2	Assumed
Ambient temperature	11.5±0.5	C	Measured
Density of fresh water (ρ_w)	1000	kg/m^3	Calculated equation of state from [54]
Density of unprepared gelatin	1350	kg/m^3	Available literature value for bovine gelatin [55]
Dynamic viscosity of fresh water (μ_w)	0.001	Pa s	Calculated, ambient equation in [56]
Gelatin concentration by mass	2.00	%	Measured
Gel width (w_g)	16	cm	Measured
Wave period (T)	0.75	s	Measured

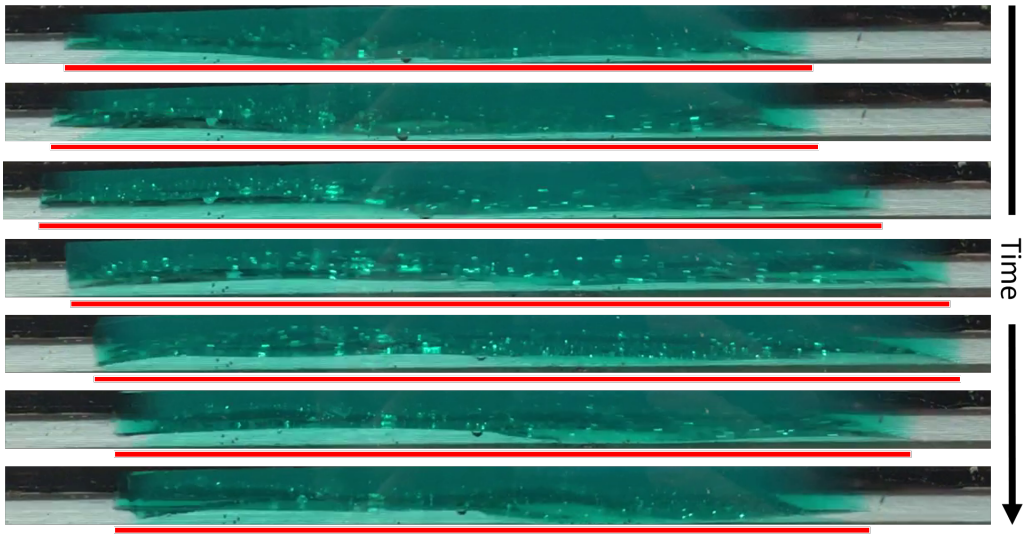

Figure 5.1: Still frames from Experiment D showing gel extension and contraction over the course of one wave period. Red bars indicating gel position have been added for clarity.

nusoid was fitted to data extrema. Sinusoidal fits are presented in the appendices. The amplitudes of these sinusoidal fits are used in the remaining analysis.

5.1 Properties of Gelatin

Rheological properties of the selected gelatin proved quite difficult to measure. Two-to-three millimeter thick disks of gelatin four centimeters in diameter were cast on a steel sheet in a magnetic mold. After removal of the mold, the disks were removed from the sheet into a plate of water by inverting the sheet and pouring warm water onto the exposed side. The samples were removed from the water, placed on the testing plate, and patted dry. Oscillatory rheology was measured in parallel-plate geometry on a TA Discovery HR-2 rheometer at BCRI. The plates were covered with a layer of 400-grit sandpaper to prevent slippage, and testing was conducted under constant axial force (0.1 N) to ensure consistency between samples of differing thickness. Frequency was matched to that of the relevant wave-tank experiments (1.33 Hz). Strain was controlled starting at 10% and increasing to 500%. Attempts to control strain below 10% were unsuccessful. Analysis of the strain-sweep results are presented in Figure 5.5.

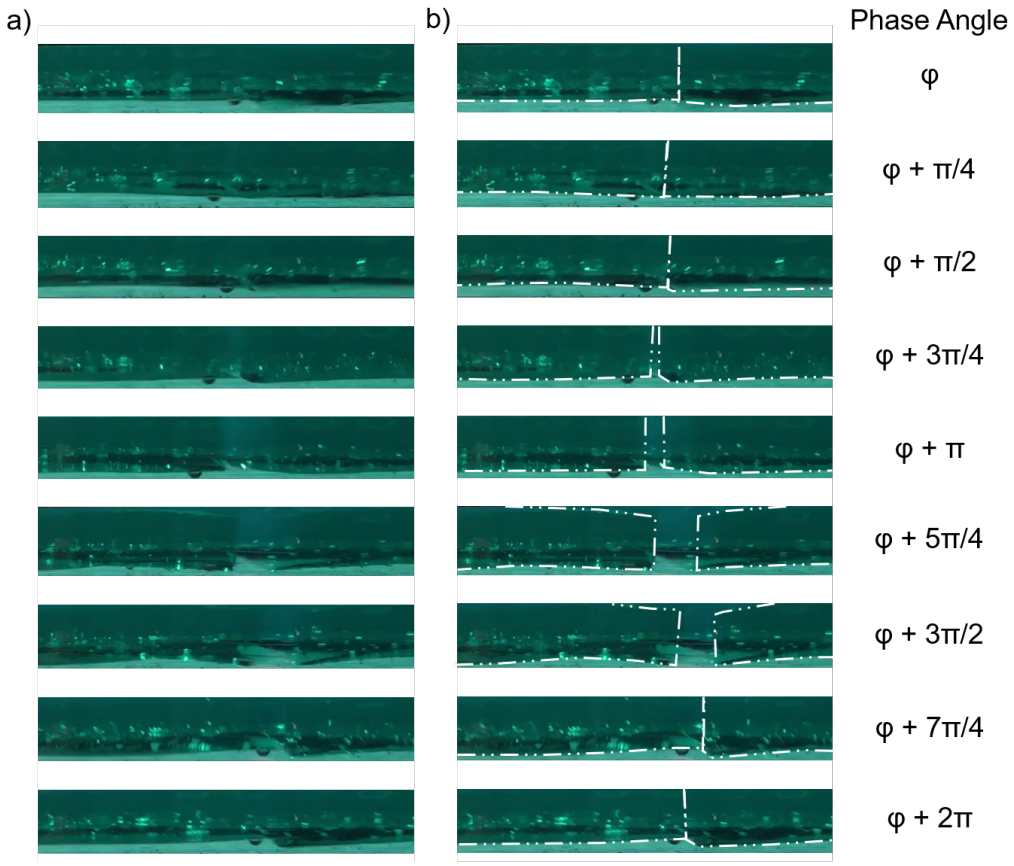

Figure 5.2: Still frames from Experiment D. (a) shows crack extension and contraction over one wave period, with crack boundaries highlighted in (b).

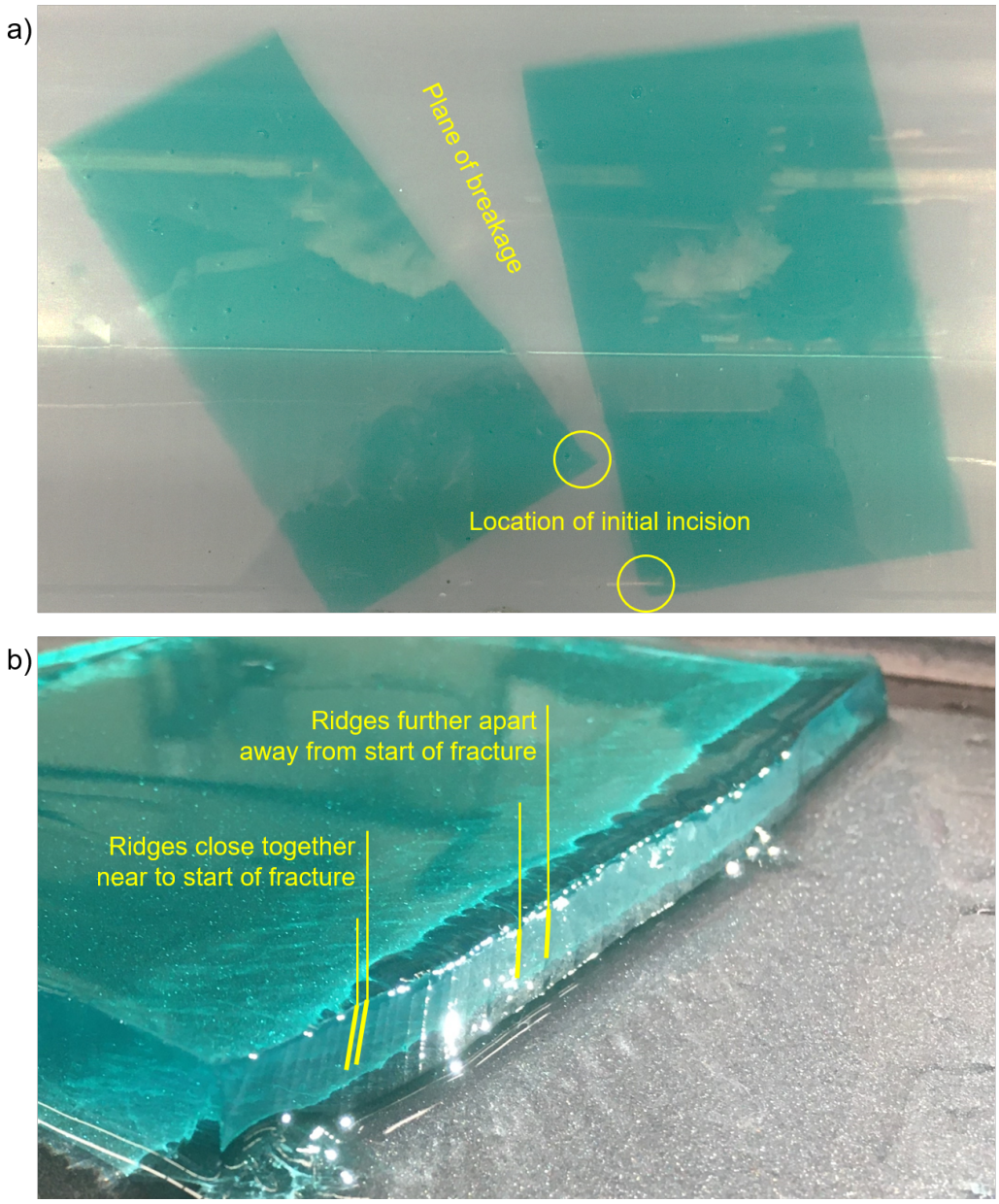

Figure 5.3: Photographs from Experiment D. (a) shows the gel after breakage and (b) provides a closer image of the left gel fragment from (a). Striations in (b) are indicative of breakage over a given wave cycle. Two sets of striations have been highlighted in yellow. Crack extension occurs slowly early on, indicated by the small gaps between ridges on the left side of (b), but increases in speed over time.

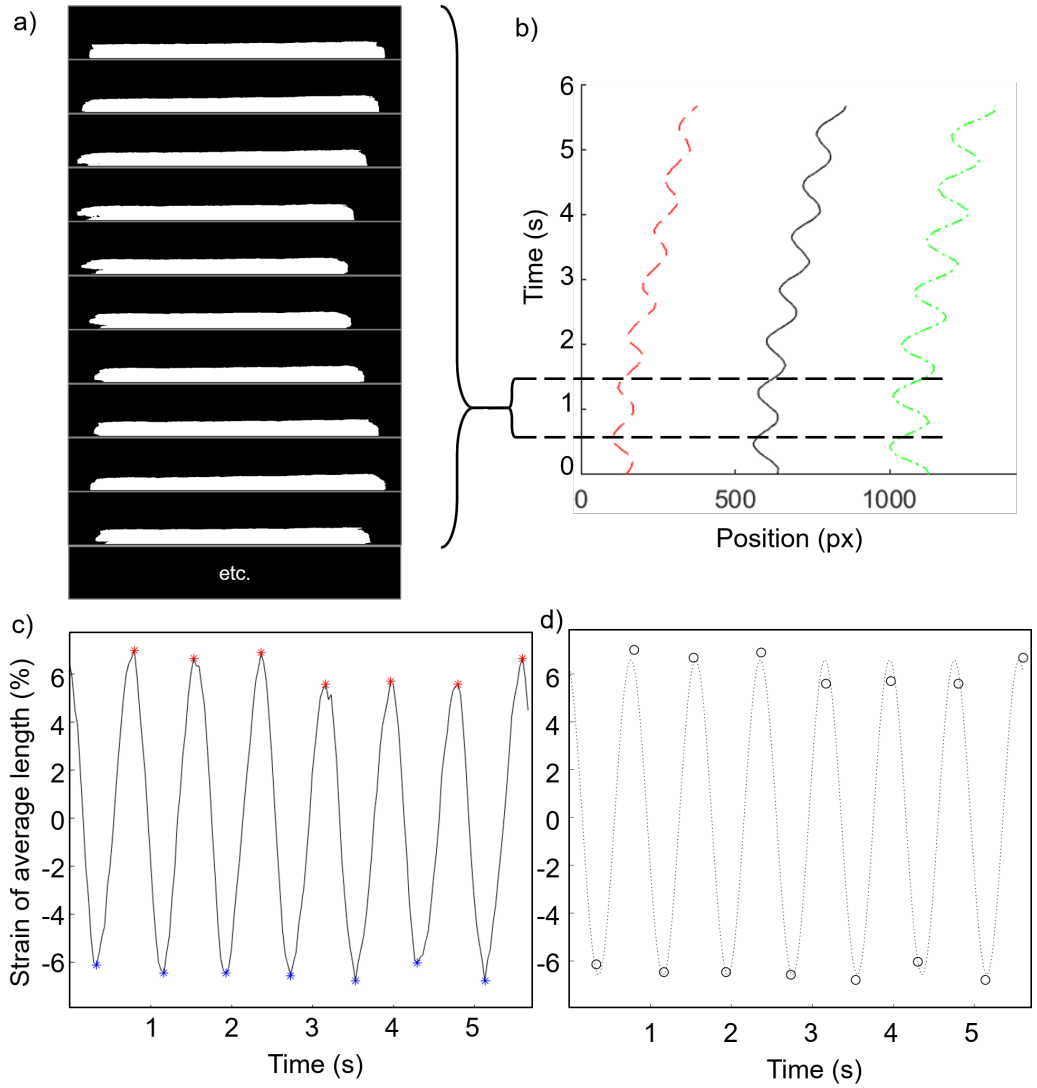

Figure 5.4: Analysis of data from Experiment C. Experimental footage (as in Figure 5.1) is processed to isolate gel location in each frame (a). Endpoints and centroid locations are then isolated (b), presented as coloured and black lines respectively. Strain is calculated (c) with respect to average length, with peak and trough locations noted as asterisks in (c) and circles in (d). Finally, peak and trough data is fitted to a sinusoid (d), of which the amplitude is used for comparison with analytical models.

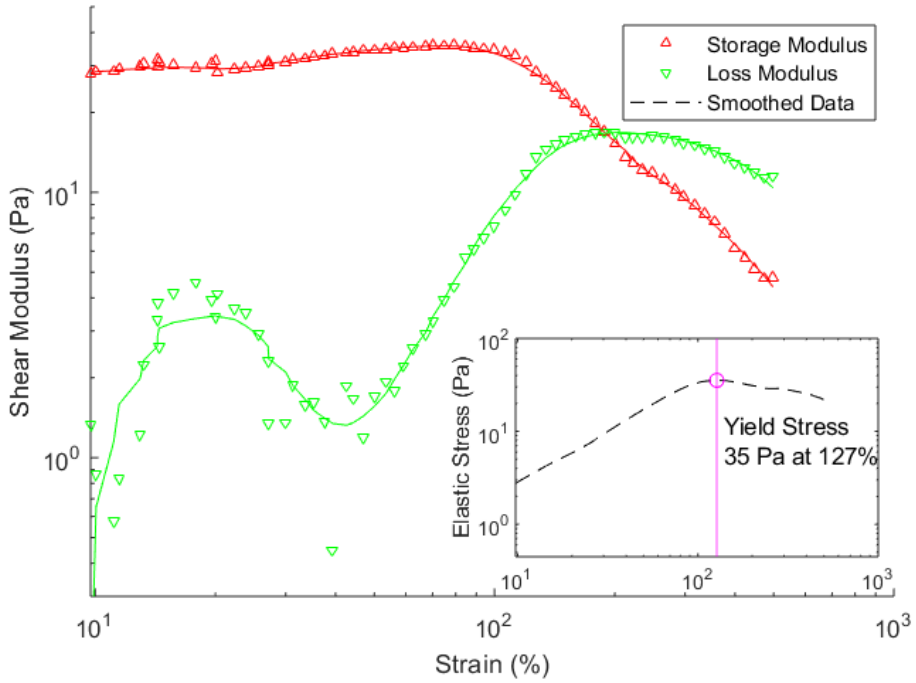

Figure 5.5: Rheological analysis of gelatin prepared at 2% weight concentration using an oscillatory strain experiment. Inset shows yield stress calculation using the methodology of [39]. Testing conducted at 11°C at 1.33 Hz. Two additional tests were run, which provided results of the same order of magnitude. Yield stress calculation was performed on smoothed data.

Yield stress measured in the three analyses were 23, 25, and 45 Pa at strain values of 130, 127, and 160% using the elastic stress method. The elastic yield stress calculated as shown in Figure 5.5 (35 Pa) will be used for analysis, both because it provided yield-stress results in between those from other tests and because there were no complicating factors surrounding sampling.

5.2 Analysis of experimental data: strain

As strain could not be related to resting gel length using video data due to issues of perspective and recording interval, strain is presented in comparison to gel mid-length (ε_m) instead of resting-length (ε). This recasting of strain may be completed using Equation 5.1, where $\bar{\varepsilon}$ is average strain.

$$\varepsilon_m = \frac{\varepsilon - \bar{\varepsilon}}{1 + \bar{\varepsilon}} \tag{5.1}$$

Values for Young's modulus and viscosity were calculated using Equations 2.22, 2.23, 2.25, and 2.26 from the closest oscillatory rheology data ($G' = 28.5$ and $G" = 0.6$, Figure 5.5). Equations 3.12 and 3.13 were used to calculate strain for time after decay of exponential terms, recast with a mid-length reference using Equation 5.1. Results are presented in Figure 5.6.

As there is a fairly even spread of longer- and shorter-wave experiments visible in Figure 5.6, it is fairly safe to conclude that wave length ratio, and not wave length, is the driving parameter in experimentation. A number of factors could be contributing to the spread of data, ranging from wave height to inconsistency in gelatin preparation. The only particularly glaring outlier is the longest gel: in this experiment, there was considerable interaction between the gel and the mesh, potentially introducing non-negligible gel-mesh friction effects.

While the Maxwell and Kelvin-Voigt models significantly under-predict strain, the degree is predictable; multiplying results by a constant factor results in a good match. A comparison between the predicted and experimental strain is shown in Figure 5.7.

Understanding that the models explain a constant proportion of the experimental strain, one may note that the model and data trends are almost a perfect match. For a given wave system, this trend is a function of the non-dimensional half-length: the absolute-value portion of 4.3. Looking at this trend can give an idea of what gel lengths will be the most and least stable in a given wave system. This trend is explored more in Figure 5.8.

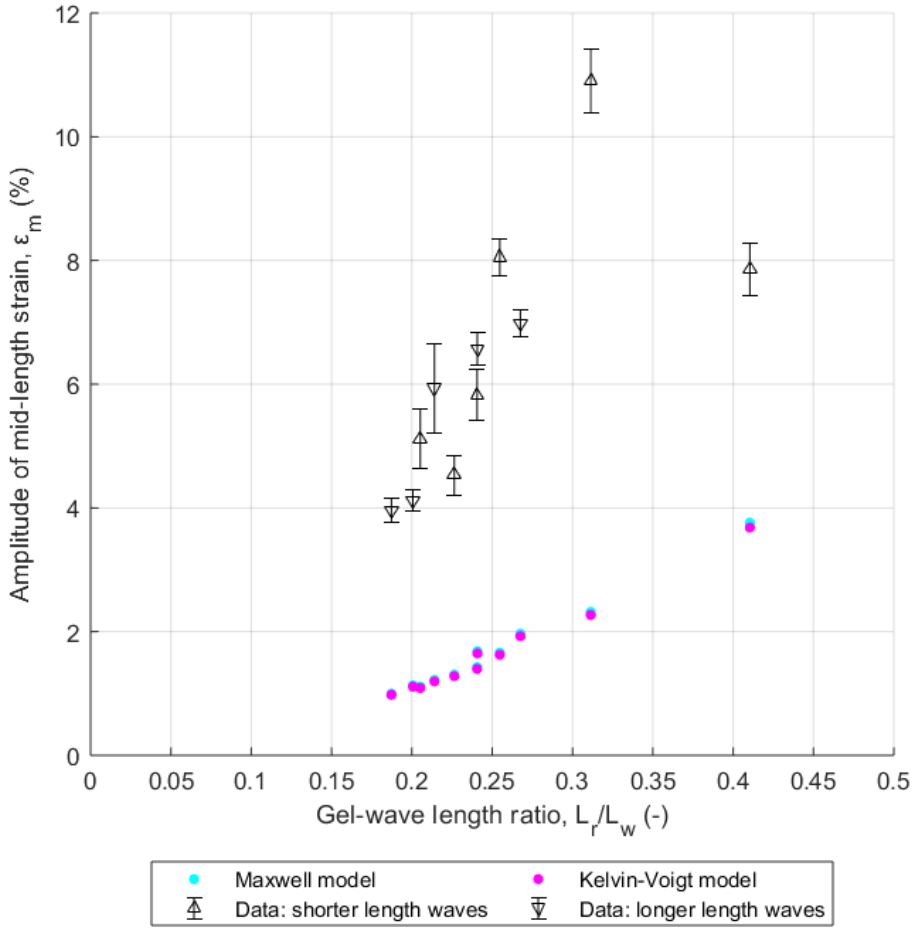

Figure 5.6: A comparison of gel model results to experimental data. Experimental data for the two wavelengths tested are differentiated with triangles. Model results are presented with coloured dots. Results of the Maxwell model are mostly obscured by those of the Kelvin-Voigt model.

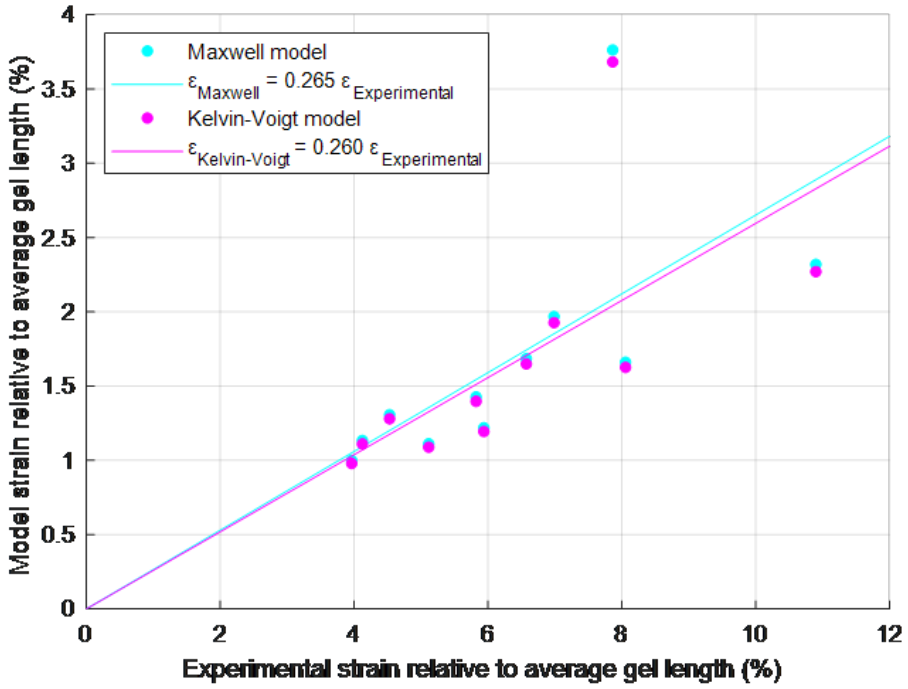

Figure 5.7: Performance of analytical models in comparison to experimental data. Analytical models tend to under-predict gel strain by a constant factor. Standard errors of approximation are both ~0.03%.

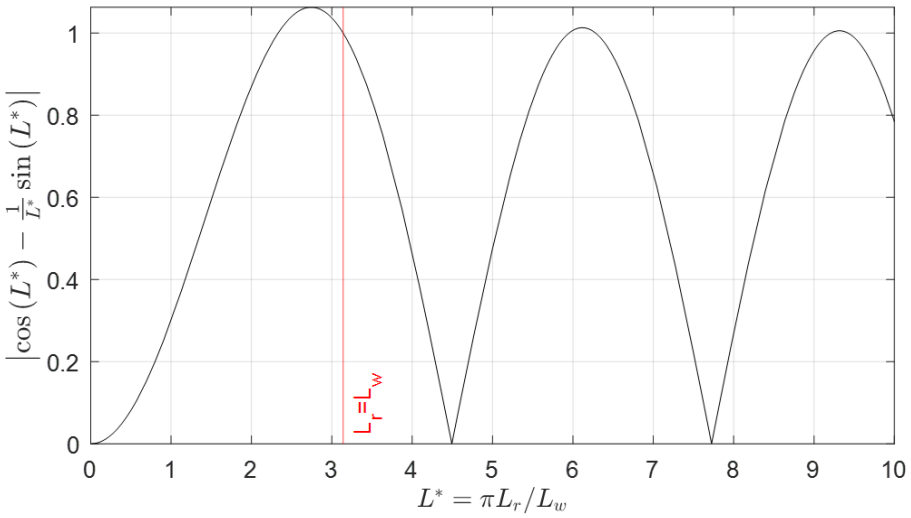

Figure 5.8: The key trend visible in strain models.

Interestingly, gel strain peaks where gel length is a multiple of the wavelength, where deviation decreases with increasing L^*. To explain this, consider where the gel and wavelengths are equal: one half of the wave will pull to the left and the other wave will pull to the right, maximizing strain.

5.2.1 Potential causes for deviation between theoretical and experimental results

This study investigated a phenomenon which was, until now, unexplored in literature. As such, it is only natural that the fairly simplistic model explored here brings up additional questions. What would cause the models to so severely underestimate the experimental response? This section explores this question.

The first question is whether the velocity-ratio assumption was valid. Recall that the equations derived here assume that the gel is not advecting. Following Equation 4.5, we find $6\% < u_{g,max}/U < 7\%$ for the range of parameters explored in experimentation. While this indicates that the models will experience some degree of inaccuracy due to gel drift, the scale of this inaccuracy is low enough that one would not expect it to cause a major error in approximation.

The second question is what additional impact the mesh had. The behaviour of the velocity field underneath the mesh was not quantified, and the impact was

almost certainly not a simple, fractional reduction in stress. The impact of the mesh, however, was likely a *reduction* in the force on the gel instead of an increase. As such, the mesh is unlikely to be the main confounding factor in the models' underestimation of experimental results.

The third question is what other forces may be at play. While attempts to incorporate inertia were made by the author, the trends exhibited by inertial models did not match experimental results. This is likely because inertia cannot be incorporated into such a system alone: other forces, such as pressure, may also be significant. Pressure impacts likely also explain the discrepancy between model and experimental results.

The initial assumption of an invariable stress field may also be brought into question. According to more traditional boundary layer theory, the boundary layer thickness at the toe of a finite plate is zero, increasing in size along the plate [57]. Perhaps something similar could be happening here. In a similar vane, a wake behind the gel could also disrupt predictions. Determining these effects, however, requires an understanding of wave boundary layers around a plate considerably beyond the scope of this preliminary study.

5.3 Analysis of experimental data: breakage stress

While strain is caused by spatial average stress, breakage will be determined by the cross-sectional stress at the location of breakage; in this case, at the centroid. Figure 5.9 shows which experiments broke, aligned with the predicted centroidal stress from Equation 4.4. In order to account for the additional strain seen in experiments, centroidal stress has been scaled according to the factors derived in Figure 5.7.

While one gel sample broke early, probably due to imprecision in transfer or crack placement, Figure 5.9 shows a clear threshold stress for breakage, approximately 5 Pa. This is considerably lower than the oscillatory yield stress (35 Pa), indicating that failure is due to fatigue. This conclusion is supported by the striations observed along the fracture. Unfortunately, due to laboratory closures associated with the COVID-19 pandemic, this could not be verified with stress-threshold testing; but a potential method for predicting the breakage stress is presented in the appendices.

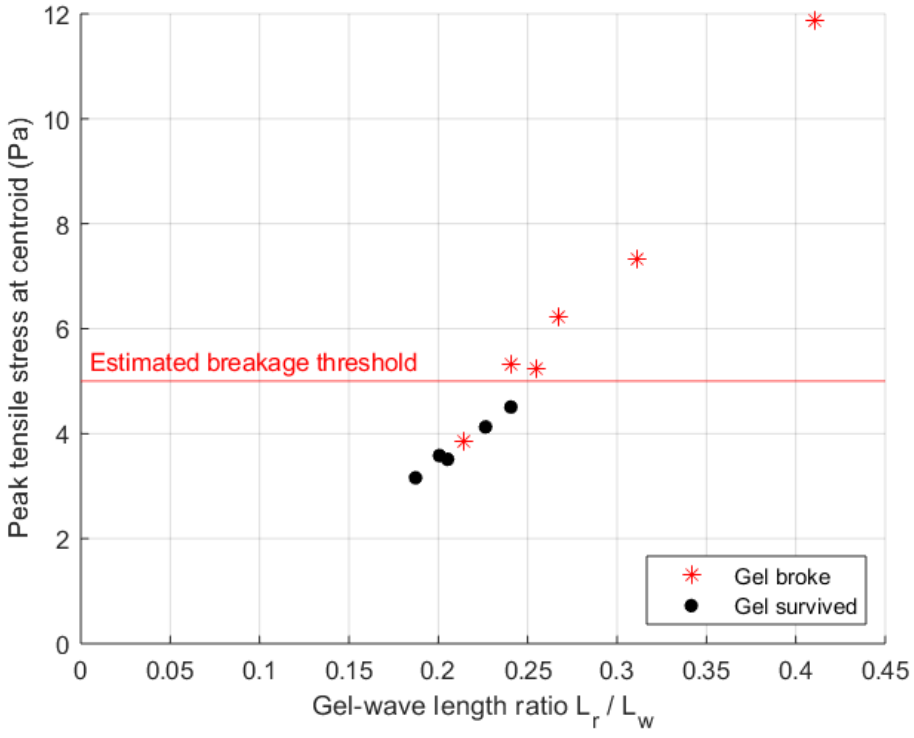

Figure 5.9: Experimental results highlighting occurrence of gel breakage. Data indicates the clear presence of a strain threshold, approximated as 5 Pa.

5.4 Implications for spill response

The next step is to consider what this study tells us about potential real-world applications of gellants. Could a shear-gradient alone cause the breakage of a marine surface gel, disregarding such factors as wave-induced bending?

The real world is considerably more complex than a wave tank. In a true marine situation, wind waves occur in a range of intermixed heights and frequencies depending on such factors as wind speed, distance from land, and wind duration. Not all these waves are linear, either: as wind speeds increase, the water surface becomes more and more covered by isolated breaking waves ("white horses"). In nautical circles, wave conditions serve as a reliable indicator for wind speed via the Beaufort Scale. This wind-classification scale was invented in the early 1800s, adopted by the Royal Navy in 1838 [58]. As this study is concerned only with linear waves, applicability of conclusions to breaking wave conditions is not suggested. While an oil gel may well survive a gently spilling breaker, it is suggested that models be limited to winds below 5 m/s, covering the first four levels of the Beaufort Scale. While isolated breakers do occur in a Beaufort 4 wind (gentle breeze), white horses only become frequent at "moderate breeze" levels and above.

Wave fields in the open ocean are neither monochromatic nor unidirectional. Rather, waves at a range of amplitudes and frequencies interfere to produce a given wave field. Fortunately, wind generates waves in a fairly predicable manner, and so a wave field may be characterized using a single wave of given period and height. The wave period of choice, T_p, represents the most common wave frequency occurring in a wave field. The typical wave height used for characterization is termed the "significant wave height", or H_{m0}. The definition of significant wave height has gone through a few iterations over the years, with the current definition related to the zeroth moment of a wave spectrum [30]. This value is fairly close to the average height of the highest third of the waves (the older definition), and the wave height as estimated by an observer [30].

As outlined in the *Coastal Engineering Manual* using SI conventions [30], wind (U_{10}, velocity typically measured at 10 m elevation) applies a stress on the water surface, characterized as a "friction velocity" (u_*)

$$u_* = \sqrt{0.001U_{10}^2(1.1+0.035U_{10})} \tag{5.2}$$

which may be used to calculate T_p and H_{m0}. In fully developed wave conditions [30],

$$\frac{gH_{m0}}{u_*^2} = 2.115 \times 10^2 \tag{5.3}$$

Stress above and beyond that caused by

$$\frac{gT_p}{u_*} = 2.398 \times 10^2 \tag{5.4}$$

This allows peak stress to be calculated from wind speed, noting that $\tanh(kd) \approx 1$ for deep water. The quantity k may be calculated from T_p using the deep-water dispersion relation $k_p = 4\pi^2 g^{-1} T_p^{-2}$.

Consider the case of a fairly thick oil slick: this could be from rapid gellant application or the herder-induced slick thickening. Large-scale trials in the Barents Sea showed existing herders were quite capable of achieving slick thicknesses of 4 mm or more [20], so let us use 4 mm for the thickness of our hypothetical gel. This will preserve the slick at a thickness sufficient for an in-situ burn [20], assuming the gelled oil is still combustible, with increased structural integrity than in a thinner gel. Assume a stress threshold of 5 Pa, as has been found above.

Interestingly, Figure 5.10 shows that the impact of cyclic stretching tends to decrease with increasing wind speed. This is because the gel length is sufficiently shorter than the wave length, so stretching will be minimal. At these higher wind speeds, breakage will likely be caused by some factor other than stretching induced by spatial velocity gradients. Successful gelling of the oil will preserve the oil in-situ, potentially increasing the effectiveness of other, slower-to-implement remediation techniques such as skimming. This time could also be used by regulators to thoughtfully consider the use of burning as a remediation technique, which requires regulatory approval on a case-by-case basis [11].

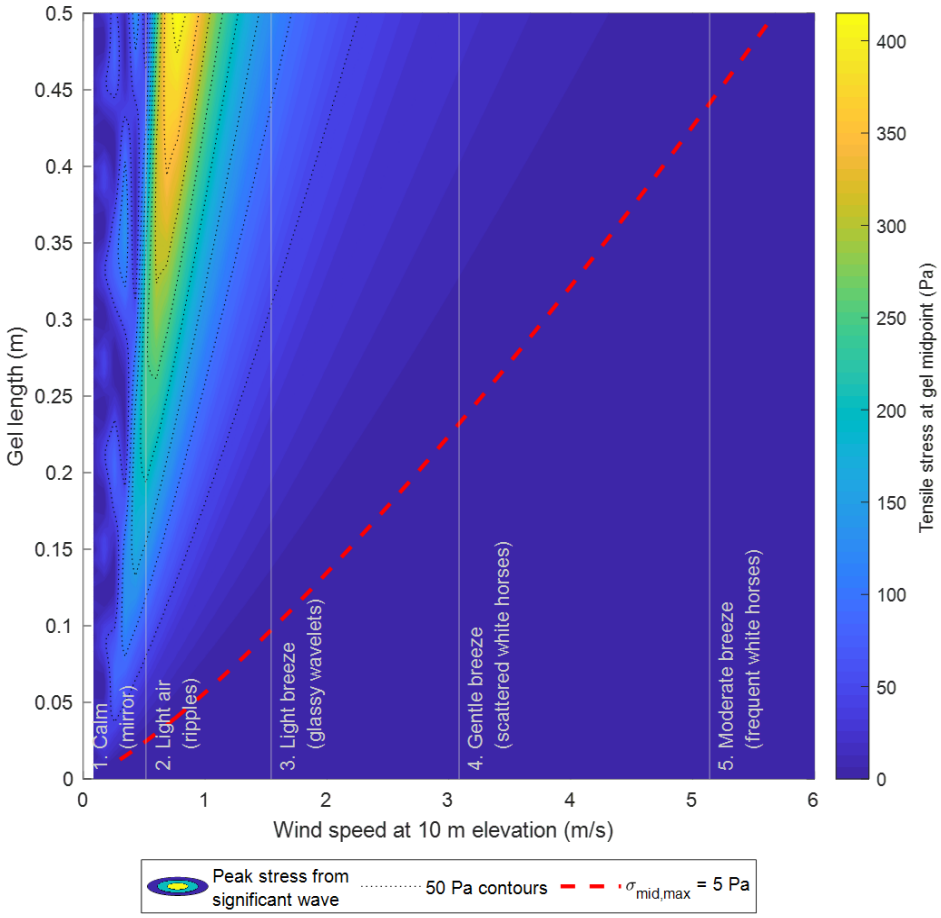

Figure 5.10: Applicability of a hypothetical gelling agent for lengths up to 2 m. Maximum tensile stress at mid-length of a 4 mm thick gel is presented for significant waves of peak frequency, predicted for various wind speeds. The assumed breakage stress of 5 Pa is marked with a red dashed line along its primary contour and 50 Pa contours are noted with dotted lines.

Chapter 6

Conclusions

6.1 Summary

The objective of this research was to explore the wave-induced stretching and breakage behaviour of marine surface gels through experimentation and analytical modeling. This topic, hitherto unexplored in literature, exists at an intersection of several fields, including hydraulic, material, and spill sciences, and requires some knowledge from all these fields to truly understand.

Chapter 1 provides the reader with some background into oil spills and their cleanup. Continued global demand for oil means a continued threat of marine spills, and oil spills can be disastrous for marine life. When oil is introduced into the environment it goes through a number of changes, known as weathering. Some of the more important weathering processes to consider in remediation include spreading, evaporation, emulsification, and dispersion. While some of these processes contribute to the eventual breakdown of a spill, others exacerbate the issue and frustrate efforts at remediation. A number of remediation techniques have been developed to clean up oil spills, both physically and chemically. One class of chemical spill treating agents, gellants, has recently resurfaced as a way to contain a spill until other remediation techniques can be mobilized.

Chapter 2 discusses gels and how wave-induced horizontal velocity gradients might cause them to break. Gels are solid-like materials made up of a liquid supported by a structural component, where the liquid forms the vast majority of the volume. They do not truly behave as solids or fluids, but must instead by studied through a rheological lens. Phase-selective Low Molecular Weight Organogelators are a type of supramolecular gellant showing particular promise for oil spill remediation. These chemicals, which would typically exist as small, distinct particles, build up to form complex lattice structures when exposed to specific stimuli. Interstitial space in these networks is taken up by oil preferentially over water. From a mathematical standpoint, there are a few ways to describe rheological materials. These include the Maxwell and Kelvin-Voigt models, which can be written using different combinations of springs and dashpots. Tensile stresses on a marine

surface gel induced by wave-related horizontally variable velocity gradients were proposed as a potential failure mechanism.

Chapter 3 delves into the mathematics of how gels interact with a wave-induced velocity gradient. Generalizing a modified solution to Stokes' Second Problem allows a stress-field approach to determining key forces acting on a gel. This type of approach is valid if advection of the gel is low and strain is not too great. Applying this stress field to mathematical gel descriptions allowed the development of new models for gel behaviour under influence of linear wave action. These analytical models, derived separately for simple elastic, Maxwell, and Kelvin-Voigt materials, predict gel strain as a sinusoidal function of time.

Chapter 4 outlines a novel method for testing gel behaviour in waves: bottom-of-tank experimentation. By placing a dense gel at the bottom of a wave tank, one may completely isolate linear strain effects from wave-induced bending. Wave tanks at both UBC and BCRI were considered, with their advantages and disadvantages outlined. The UBC wave tank was selected for bottom-of-tank experimentation, with gelatin as the gel of choice. Theory derived in Chapter 3 was modified to address the bottom-of-tank experimental setup.

Chapter 5 provides a discussion of findings from experiments at UBC. While the trend predicted by the derived analytical models matches experimental data, the models under-predict strain by a constant factor. Additional strain is likely due to other forces, such as pressure. Breakage occurred when stress exceeded a certain threshold. As this threshold was considerably lower than the yield stress, breakage is likely due to fatigue. Analyzing peak stress in natural wave fields showed that marine surface gels are least resistant to short waves associated with low wind speeds, at least from the perspective of tensile stresses resulting from wave-induced shear-stress gradients.

6.2 Future work

Prior to this study there was little extant literature on the interactions between surface gels and ocean waves. As this thesis is at the forefront of inquiry, there is considerable room for further research. In order to better understand the implications of bottom-of-tank experimentation, investigators should:

- expand analytical models to account for additional forces such as pressure and inertia,

- repeat experiments using a broader range of gels with better-quantified properties, and
- consider taking advantage of bubble accumulation to test a model gel both at depth and on the water surface.

This study has also noted some broader literature gaps which should be addressed, including:

- how wave-induced bending might cause the breakage of a marine surface gel,
- how breaking waves interact with a marine surface gel,
- characterization of oscillatory flows around a freely-advecting plate, and
- vertical transmission of a linear wave through a horizontal mesh.

Oil spills are an ever-present threat to the marine environment, and we must do our part to ensure their impact is as low as possible.

Bibliography

[1] REN21, "Renewables 2019: Global status report," *REN21 Secretariat*, 2019.

[2] International Energy Agency, *Oil 2020: Analysis and Forecast to 2025*. 2020.

[3] International Tanker Owners Pollution Federation, "Oil tanker spill statistics 2019," London, Jan 2020.

[4] "barrel of oil equivalent," 2002.

[5] C. Robertson and C. Krauss, "Gulf spill is the largest of its kind, scientists say," *The New York Times*, vol. 2, no. 8, 2010.

[6] M. Fingas, *The basics of oil spill cleanup*. CRC press, 2012.

[7] Canadian Association of Petroleum Producers, "2019 crude oil forecast, markets and transportation," 2019.

[8] T. L. King, B. Robinson, F. Cui, M. Boufadel, K. Lee, and J. A. Clyburne, "An oil spill decision matrix in response to surface spills of various bitumen blends," *Environmental Science: Processes & Impacts*, vol. 19, no. 7, pp. 928–938, 2017.

[9] L. Mu, L. Wang, and J. Yan, *Information Engineering of Emergency Treatment for Marine Oil Spill Accidents*. CRC Press, 2019.

[10] Transport Canada, "Roles and responsibilities," Sep 2018.

[11] BC Ministry of Environment, *British Columbia Marine Oil Spill Response Plan*. 2013.

[12] D. Scholz, J. Kucklick, R. Pond, A. Walker, A. Bostrom, and P. Fischbeck, "Fate of spilled oil in marine waters: Where does it go, what does it do, and how do dispersants affect it," *Prepared by Scientific and Environmental*

Associates, Inc., Cape Charles, VA. Prepared for the American Petroleum Institute, Washington, DC. API Publ, vol. 4691, p. 43, 1999.

[13] G. Hum and H. Hamza, *Strategies for Mitigating the Impact of Dilbit Released into Marine Environments*. 2016.

[14] J. Hartogs, "Three years after BP oil spill, active clean-up ends in three states," *CBS News*, Jun 2013.

[15] J. A. Fay, "The spread of oil slicks on a calm sea," in *Oil on the Sea*, pp. 53–63, Springer, 1969.

[16] M. Zeinstra-Helfrich, W. Koops, and A. J. Murk, "Predicting the consequence of natural and chemical dispersion for oil slick size over time," *Journal of Geophysical Research: Oceans*, vol. 122, no. 9, pp. 7312–7324, 2017.

[17] A. Venosa and E. Holder, "Biodegradability of dispersed crude oil at two different temperatures," *Marine pollution bulletin*, vol. 54, no. 5, pp. 545–553, 2007.

[18] S. C. Johannessen, C. W. Greer, C. G. Hannah, T. L. King, K. Lee, R. Pawlowicz, and C. A. Wright, "Fate of diluted bitumen spilled in the coastal waters of British Columbia, Canada," *Marine pollution bulletin*, vol. 150, p. 110691, 2020.

[19] C. E. Brown, B. Fieldhouse, T. C. Lumley, P. Lambert, and B. P. Hollebone, "Environment Canada's methods for assessing oil spill treating agents," in *Oil Spill Science and Technology*, pp. 643–671, Elsevier, 2011.

[20] I. Buist and J. Fritt-Rasmussen, "Research summary: Herding surfactants to contract and thicken oil spills for in-situ burning in arctic waters," 2015.

[21] M. F. Fingas, *A review of literature related to oil spill dispersants especially relevant to Alaska*. Citeseer, 2008.

[22] C. McKenna, "Regulations establishing a list of spill-treating agents (Canada oil and gas operations act)," *Canada Gazette*, vol. 150, Jun 2016.

[23] F. L. Motta, S. R. Stoyanov, and J. B. Soares, "Application of solidifiers for oil spill containment: A review," *Chemosphere*, vol. 194, pp. 837–846, 2018.

[24] V. A. Mallia, D. L. Blair, and R. G. Weiss, "Oscillatory rheology and surface water wave effects on crude oil and corn oil gels with (r)-12-hydroxystearic acid as gelator," *Industrial & Engineering Chemistry Research*, vol. 55, no. 4, pp. 954–960, 2016.

[25] K. Nishinari, "Some thoughts on the definition of a gel," in *Gels: Structures, Properties, and Functions*, pp. 87–94, Springer, 2009.

[26] J. Zhang, Y. Hu, and Y. Li, *Gel Chemistry: Interactions, Structures and Properties*, vol. 96. Springer, 2018.

[27] G. Yu, X. Yan, C. Han, and F. Huang, "Characterization of supramolecular gels," *Chemical Society Reviews*, vol. 42, no. 16, pp. 6697–6722, 2013.

[28] X. Yu, L. Chen, M. Zhang, and T. Yi, "Low-molecular-mass gels responding to ultrasound and mechanical stress: towards self-healing materials," *Chemical Society Reviews*, vol. 43, no. 15, pp. 5346–5371, 2014.

[29] Y. Wang, Y. Wang, X. Yan, S. Wu, L. Shao, Y. Liu, and Z. Guo, "Toluene diisocyanate based phase-selective supramolecular oil gelator for effective removal of oil spills from polluted water," *Chemosphere*, vol. 153, pp. 485–493, 2016.

[30] United States Army Corps of Engineers, *Coastal engineering manual*. US Army Corps of Engineers, 2002.

[31] A. Toffoli and E. M. Bitner-Gregersen, "Types of ocean surface waves, wave classification," *Encyclopedia of Maritime and Offshore Engineering*, pp. 1–8, 2017.

[32] S. Chandrasekaran, *Dynamic analysis and design of offshore structures*. Springer, 2015.

[33] K. Praveen, D. Karmakar, and C. G. Soares, "Influence of support conditions on the hydroelastic behaviour of floating thick elastic plate," *Journal of Marine Science and Application*, vol. 18, no. 3, pp. 295–313, 2019.

[34] A. Y. Malkin and A. I. Isayev, *Rheology: concepts, methods, and applications*. Elsevier, 2017.

[35] G. Papanicolaou and S. Zaoutsos, "Viscoelastic constitutive modeling of creep and stress relaxation in polymers and polymer matrix composites," in *Creep and fatigue in polymer matrix composites*, pp. 3–59, Elsevier, 2019.

[36] J. van Otterloo and A. R. Cruden, "Rheology of pig skin gelatine: Defining the elastic domain and its thermal and mechanical properties for geological analogue experiment applications," *Tectonophysics*, vol. 683, pp. 86–97, 2016.

[37] M. Dinkgreve, J. Paredes, M. M. Denn, and D. Bonn, "On different ways of measuring "the" yield stress," *Journal of non-Newtonian fluid mechanics*, vol. 238, pp. 233–241, 2016.

[38] G. Ovarlez, "Rheometry of visco-plastic fluids," in *Lectures on Visco-Plastic Fluid Mechanics*, pp. 127–163, Springer, 2019.

[39] H. Walls, S. B. Caines, A. M. Sanchez, and S. A. Khan, "Yield stress and wall slip phenomena in colloidal silica gels," *Journal of Rheology*, vol. 47, no. 4, pp. 847–868, 2003.

[40] H. Schlichting and K. Gersten, *Boundary-Layer Theory*. Berlin, Heidelberg: Springer Berlin Heidelberg, 9th 2017.;ninth;9th 2017; ed., 2017.

[41] P. Nielsen, *Coastal bottom boundary layers and sediment transport*, vol. 4. World scientific, 1992.

[42] A. Mujal-Colilles, J. M. Mier, K. T. Christensen, A. Bateman, and M. H. Garcia, "PIV experiments in rough-wall, laminar-to-turbulent, oscillatory boundary-layer flows," *Experiments in fluids*, vol. 55, no. 1, p. 1633, 2014.

[43] H. Li *et al.*, "Stability of oscillatory laminar flow along a wall," 1954.

[44] C.-C. Huang, P.-Y. Chen, and C.-C. Shih, "Estimating the viscoelastic modulus of a thrombus using an ultrasonic shear-wave approach," *Medical physics*, vol. 40, no. 4, p. 042901, 2013.

[45] B. Guillouzouic, "D2. 12 collation of wave simulation methods," *Energy Research Centre of the Netherlands (ECN), Institute for Technological Research (IPT), Plymouth University, Queen's University Belfast, The French Research Institute for Exploitation of the Sea (IFREMER), University College Cork, and University of Edinburgh*, p. 85, 2014.

[46] Y. Ouellet and I. Datta, "A survey of wave absorbers," *Journal of hydraulic research*, vol. 24, no. 4, pp. 265–280, 1986.

[47] R. Schrieber and H. Gareis, *Gelatine handbook: theory and industrial practice*. John Wiley & Sons, 2007.

[48] Z. Wang, B. Liang, and G. Wu, "Experimental investigation on characteristics of sand waves with fine sand under waves and currents," *Water*, vol. 11, no. 3, p. 612, 2019.

[49] M. Patarapanich, "Forces and moment on a horizontal plate due to wave scattering," *Coastal Engineering*, vol. 8, no. 3, pp. 279–301, 1984.

[50] K.-U. Graw, "The submerged plate as a wave filter the stability of the pulsating flow phenomenon," in *Coastal Engineering 1992*, pp. 1153–1160, 1993.

[51] X. Yu, "Functional performance of a submerged and essentially horizontal plate for offshore wave control: a review," *Coastal engineering journal*, vol. 44, no. 02, pp. 127–147, 2002.

[52] A. Onder and J. Yuan, "Turbulent dynamics of sinusoidal oscillatory flow over a wavy bottom," *Journal of Fluid Mechanics*, vol. 858, pp. 264–314, 2019.

[53] D. G. Grigoriadis, A. A. Dimas, and E. Balaras, "Large-eddy simulation of wave turbulent boundary layer over rippled bed," *Coastal engineering*, vol. 60, pp. 174–189, 2012.

[54] A. E. Gill, *Atmosphere - ocean dynamics*. Elsevier, 2016.

[55] B. R. Frieberg, R.-S. Garatsa, R. L. Jones, J. O. Bachert, B. Crawshaw, X. M. Liu, and E. P. Chan, "Viscoplastic fracture transition of a biopolymer gel," *Soft matter*, vol. 14, no. 23, pp. 4696–4701, 2018.

[56] M. L. Huber, R. A. Perkins, A. Laesecke, D. G. Friend, J. V. Sengers, M. J. Assael, I. N. Metaxa, E. Vogel, R. Mareš, and K. Miyagawa, "New international formulation for the viscosity of h2o," *Journal of Physical and Chemical Reference Data*, vol. 38, no. 2, pp. 101–125, 2009.

[57] L. Birk, *Fundamentals of Ship Hydrodynamics: Fluid Mechanics, Ship Resistance and Propulsion*. John Wiley & Sons, 2019.

[58] F. Singleton, "The Beaufort scale of winds–its relevance, and its use by sailors," *Weather*, vol. 63, no. 2, pp. 37–41, 2008.

[59] T. Fett, *Stress intensity factors-t-stresses-weight functions*. 2008.

[60] M. A. Berthaume, "Food mechanical properties and dietary ecology," *American Journal of Physical Anthropology*, vol. 159, pp. 79–104, 2016.

[61] J. Tang, J. Li, J. J. Vlassak, and Z. Suo, "Fatigue fracture of hydrogels," *Extreme Mechanics Letters*, vol. 10, pp. 24–31, 2017.

Appendix A

Relationship between dashpots and viscosity

The following derivation accompanies Figure 2.4 in explination of why liquids exhibit stress proportional to strain rate in a dashpot model. Neglecting acceleration and following the definitions in Figure 2.4,

$$\begin{aligned}
\sum F &= 0 \\
F_1 &= \tau A_2 \\
\sigma &= \frac{A_2}{A_1}\mu_{liquid}\frac{du}{dy} \\
\sigma &= \frac{A_2\mu_{liquid}}{A_1 Y}\frac{dx}{dt} \\
\sigma &= \mu_{liquid}\frac{A_2 L}{A_1 Y}\frac{d\varepsilon}{dt} \\
\sigma &= \mu_{dashpot}\frac{d\varepsilon}{dt} \\
&\square
\end{aligned}$$

Appendix B

Sinusoidal fits of experimental data

As illustrated in Figure 5.4, sinusoids were fitted to experimental data to provide a single value for strain amplitude. Sinusoidal fits for the remaining experiments are presented here.

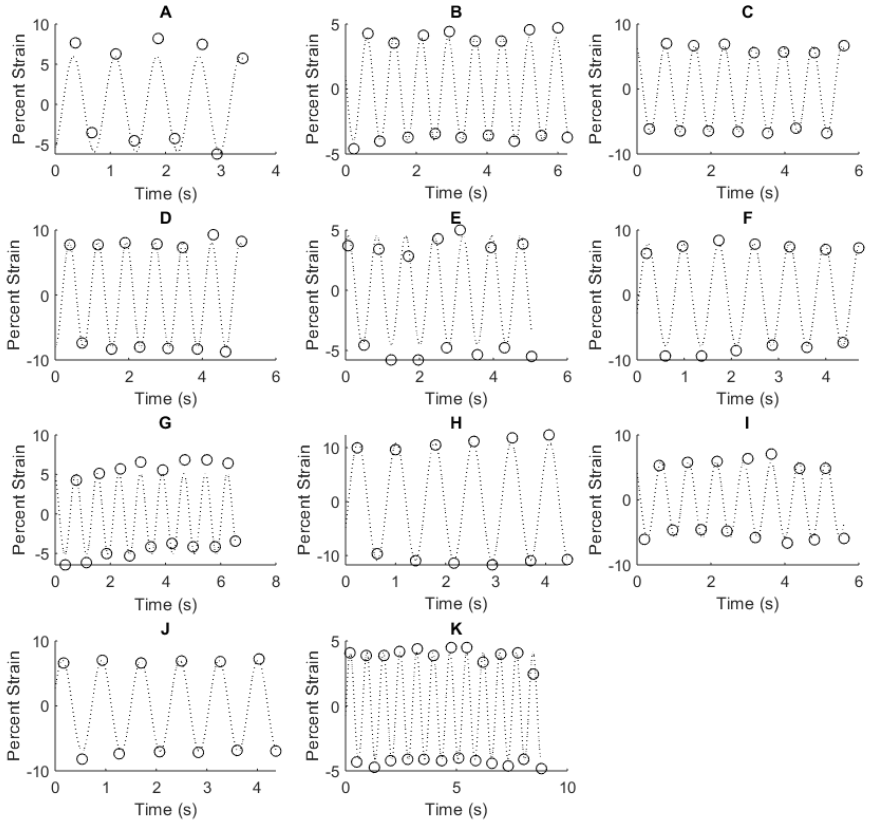

Figure B.1: Sinusoidal fits of experimental data. Sinusoids are fitted around zero, neglecting any net drift. Open circles indicate peaks and troughs in strain data. Dotted lines indicate sinusoidal fits. Sinusoidal fits are used in data analysis to quantify strain amplitude as a single value. Length of analysis interval determined based on available data.

Appendix C

Top-of-tank experimentation at BCRI

While the COVID-19 pandemic prevented a full experimental regime from taking place at BCRI, some preliminary experimentation was conducted using an early formulation of their proprietary gellant. New, better, formulations have since been produced by BCRI. Specific details of preparation will not be provided here, but the result was an irregular pattern of oil and water as the fluid portion of the gel. Experimental setup and gel irregularity are shown below. The wave absorber was constructed of kitchen sponges, as they approximate a fine horse-hair mesh.

The gel tested was 13 cm in length from the supporting bar to tailing end, 6.5 cm in width, and 1.6 mm thick. Two wave heights were examined in experimentation: 0.8 cm and 1.4 cm. Wave frequency was 1.48 Hz and water depth was 7 cm. Experimental parameters are summarized in the following table. Note that L_r here refers only gel length behind the bar.

As we do not know the impacts of bending on the gel, assume for now that bending has no impact on breakage. This will likely cause an overestimate of the importance of velocity gradient stretching, but it will do for an initial perspective on the problem.

The first set of waves was applied for 1.25 hours, during which time the gel did not break. Wave height was increased after this time. Application of the higher-amplitude waves resulted in breakage: a crack began to extend across the gel after 13 wave periods, with the gel fully broken by the 38th wave period. The threshold breakage stress, therefore, lies somewhere between the centroidal stress of the

Table C.1: BCRI experimental results

L_r (cm)	w_g (cm)	d_g (mm)	L_w (cm)	d (cm)	Frequency (Hz)	H (mm)	Duration (min)	$\sigma_{mid,max}$ (Pa)
13	6.5	1.6	50	7	1.48	8	75	4.8
						14	0.5	8.4

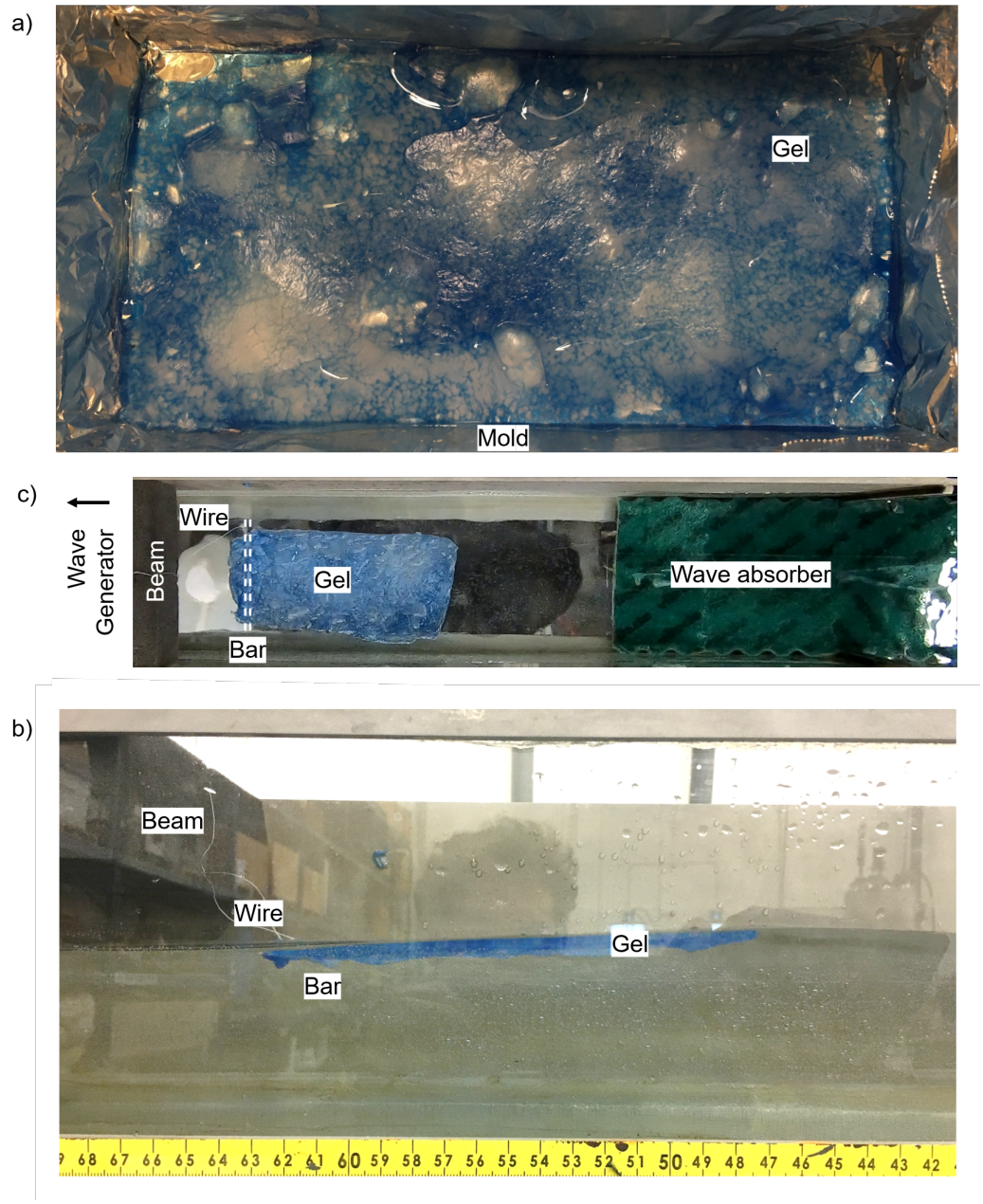

Figure C.1: Experimental setup in the tank at BC Research Inc. A diesel-water gel (a) was prepared in an aluminum mold. Areas where diesel was absorbed are dyed blue, whereas areas of water gel are white. (b) shows the gel being subjected to a low-amplitude wave. Experimental setup is shown in (c). To hold the gel in place, a mesh bar running under one end of the gel was attached to a beam over the water surface.

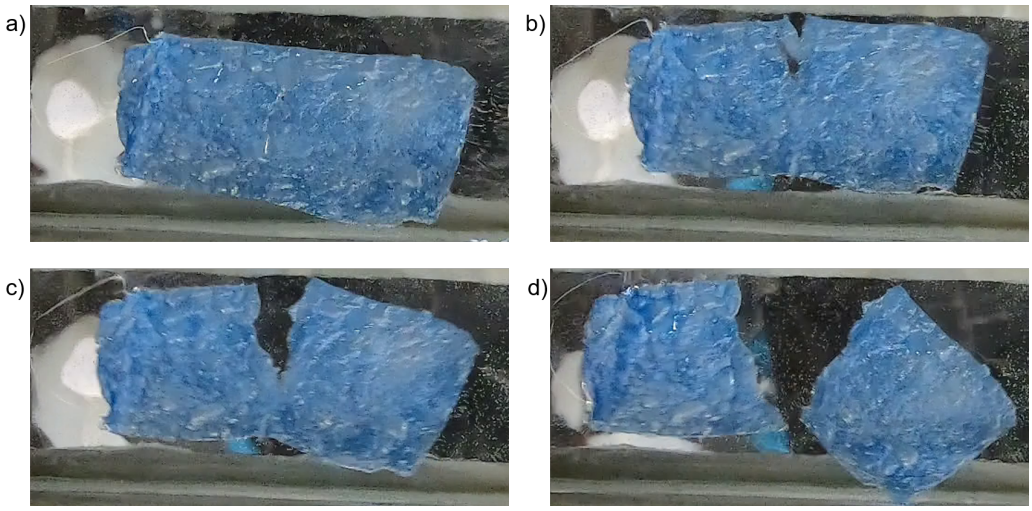

Figure C.2: Still frames from the experiment at BC Research Inc. illustrating breakage over time. Frames (a) - (d) show the gel after 4, 20, 26, and 28 wave periods.

shorter waves and that of the taller waves. The crack occurred approximately halfway along the gel.

Threshold stress for gel breakage may be calculated using 4.4, with some small modification. Assuming that horizontal velocity at the still water level is a good approximation for velocity tangential to the gel-water interface and accounting for only one side of the gel being exposed to waves, 4.4 may be written as

$$\sigma_{mid,max} = \frac{\pi H}{T \tanh(kd)} \rho_w \sqrt{\omega \nu_w} \frac{2}{k d_g} \left[1 - \cos \frac{k L_r}{2} \right] \tag{C.1}$$

As noted in the table above, we find $4.8 < \sigma_{mid,max} < 8.4$ Pa. The breakage stress threshold will therefore be at some point in this range. It is important to note that this was not the final product of gellant development; more recent iterations will have different properties.

Appendix D

Predicting the breakage threshold of a gel

As failure of the gelatin gel occurred at stresses lower than the yield stress, breakage is likely due to cyclic fatigue. Fatigue fracture is characterized by the extension of a crack through repeated loading, and may occur at applied stresses considerably less than if stress was applied continuously. Some research has been put into the fatigue failure of hydrogels, which has classified types of fracture based on the behaviour of an extending crack based on a threshold energy release rate. Unfortunately, due to COVID-19 related laboratory closures, this threshold could not be determined in this study. The science behind threshold, however, proceeds as follows.

A crack of length a in a thin, rectangular plate of length L_g and width w_g under tension (Figure 2.6) will experience a concentrated stress σ_{crack}. This concentrated stress is related to a stress intensity factor (K) by means of the geometric parameter (F_t):

$$\sigma_{crack} = \frac{K}{F_t\sqrt{\pi a}}$$

Threshold fracture energy may be related to a shear stress by way of Young's modulus and a stress intensity factor, which is dependent on geometry. For this particular case, where $a \ll w_g$, the value $F_t \approx 1.1215\,(1 - a/w_g)^{-3/2}$ is documented in literature [59]. For a plane-stress scenario, the stress intensity factor may be expressed as a function of energy release rate (Γ) [60]:

$$K = \sqrt{\Gamma E}$$

Literature has shown that, for certain gels, a crack will not extend if energy release rate is below a certain threshold value (Γ_0) [61]. This allows us to define a threshold breakage stress (σ_{break}), calculated as For a plane-stress scenario, $\Gamma_0 =$

K^2/E , so the stress threshold for breakage becomes

$$\sigma_{break} \approx \sqrt{\frac{\Gamma_0 E}{1.12^2 \pi a}}$$

In short, to predict breakage in this manner one must document two additional parameters to normal rheometric measurements: typical crack length and threshold fracture energy. This suggests that only two additional points must be quantified to predict gel breakage, beyond typical rheometric measurements: irregularity of the gel boundaries and gel fracture energy. Threshold fracture energy could be determined using cavitation rheology [55].